Author's personal copy

Deep-Sea Research II 71–76 (2012) 16–31

Contents lists available at SciVerse ScienceDirect

Deep-Sea Research II

journal homepage: www.elsevier.com/locate/dsr2

Iron from melting glaciers fuels the phytoplankton blooms in Amundsen Sea (Southern Ocean): Iron biogeochemistry

Loes J.A. Gerringa [a,*], Anne-Carlijn Alderkamp [b,c], Patrick Laan [a], Charles-Edouard Thuróczy [a], Hein J.W. De Baar [a,b], Matthew M. Mills [c], Gert L. van Dijken [c], Hans van Haren [a], Kevin R. Arrigo [c]

[a] Royal Netherlands Institute for Sea Research, PO Box 59, 1790 AB Den Burg, The Netherlands
[b] Department of Ocean Ecosystems, Energy and Sustainability Research Institute Groningen, University of Groningen, Groningen, The Netherlands
[c] Department of Environmental Earth System Science, Stanford University, USA

ARTICLE INFO

Available online 16 March 2012

Keywords:
Fe
Fe fluxes
Dissolved Fe
Total dissolvable Fe
Southern Ocean

ABSTRACT

Dissolved iron (DFe) and total dissolvable Fe (TDFe) were measured in January–February 2009 in Pine Island Bay, as well as in the Pine Island and Amundsen polynyas (Amundsen Sea, Southern Ocean). Iron (Fe) has been shown to be a limiting nutrient for phytoplankton growth, even in the productive continental shelves surrounding the Antarctic continent. However, the polynyas of the Amundsen Sea harbor the highest concentrations of phytoplankton anywhere in Antarctica. Here we present data showing the likely sources of Fe that enable such a productive and long lasting phytoplankton bloom. Circumpolar Deep Water (CDW) flows over the bottom of the shelf into the Pine Island Bay where DFe and TDFe were observed to increase from 0.2 to 0.4 nM DFe and from 0.3–4.0 to 7–14 nM TDFe, respectively. At the southern end of Pine Island Bay, the CDW upwelled under the Pine Island Glacier, bringing nutrients (including Fe) to the surface and melting the base of the glacier. Concentrations of DFe in waters near the Pine Island Glacier and the more westward lying Crosson, Dotson, and Getz Ice Shelves varied between 0.40 and 1.31 nM, depending on the relative magnitude of upwelling, turbulent mixing, and melting. These values represent maximum concentrations since associated ligands (which increase the solubility of Fe in seawater) were saturated with Fe (Thuróczy et al., 2012). The TDFe concentrations were very high compared to what previously has been measured in the Southern Ocean, varying between 3 and 106 nM. In the Pine Island Polynya, macronutrients and DFe were consumed by the phytoplankton bloom and concentrations were very low. We calculate that atmospheric dust contributed $<1\%$ of the Fe necessary to sustain the phytoplankton bloom, while vertical turbulent eddy diffusion from the sediment, sea ice melt, and upwelling contributed 1.0–3.8%, 0.7–2.9%, and 0.4–1.7%, respectively. The largest source was Fe input from the PIG, which could satisfy the total Fe demand by the phytoplankton bloom by lateral advection of Fe over a range of 150 km from the glacier. The role of TDFe as a phytoplankton nutrient remains unclear, perhaps representing an important indirect Fe source via dissolution and complexation by dissolved organic ligands (Gerringa et al., 2000; Borer et al., 2005).

© 2012 Elsevier Ltd. All rights reserved.

1. Introduction

The availability of iron (Fe) and light are the dominant factors controlling primary productivity by phytoplankton in the Southern Ocean (De Baar et al., 1990; Buma et al., 1991; Martin, 1994; Coale et al., 1996; Sunda and Huntsman, 1997). The degree of light availability is determined by latitude, seasonal changes in solar insolation and sea ice coverage, and the intensity of vertical mixing. Dissolved Fe (DFe) concentrations are controlled by dissolved organic ligands; these ligands maintain DFe at levels higher than would be expected from its low solubility in oxygenated seawater (0.1–0.4 nM Fe depending on pH, salinity and temperature, Liu and Millero, 2002).

The concentration of DFe in seawater depends on sources of Fe and the mechanisms keeping Fe in solution, as well as on processes like scavenging, precipitation, and uptake by phytoplankton that convert Fe from the dissolved into the particulate phase (Gledhill and van den Berg, 1994; Kuma et al., 1996; Rue and Bruland 1997; Croot and Johansson, 2000; Gerringa et al., 2000, 2007; Boye et al., 2001; De Baar and De Jong, 2001; Nishioka et al., 2001; Thuróczy et al., 2010, 2011; Klunder et al., 2011). The colloidal phase in the oceans is thought to be the most

* Corresponding author. Tel.: +31 222 369436.
E-mail address: Loes.Gerringa@nioz.nl (L.J.A. Gerringa).

0967-0645/$ - see front matter © 2012 Elsevier Ltd. All rights reserved.
http://dx.doi.org/10.1016/j.dsr2.2012.03.007

Author's personal copy

reactive phase, showing the largest variation with time and depth (Nishioka et al., 2003; Bergquist et al., 2007), although Kuma et al. (2000) measured the largest variations in the truly dissolved phase (<0.025 μm). Photoreduction can produce Fe(II) from dissolved colloidal Fe(III) as well as from organic complexes and particulate Fe(III) (Barbeau and Moffett, 2000; Rijkenberg et al., 2005, 2006), and may be an important factor in influencing the bioavailability of Fe for phytoplankton in the Southern Ocean (Tagliabue and Arrigo, 2006).

External sources of Fe to the Southern Ocean are limited (De Baar and De Jong, 2001; Tagliabue et al., 2010; Klunder et al., 2011). There are only a few areas where dust can enter the system, such as east of the Kerguelen plateau, Australia, and southern tip of South America (Jickells and Spokes, 2001; Blain et al., 2007; Sedwick et al., 2008). Hydrothermal sources are not known in the Southern Ocean (Tagliabue et al., 2010). Riverine input of Fe is negligible (De Baar and De Jong, 2001). Fe from the continental margins, upwelling of Fe-rich deep water and melting of sea ice and glaciers are the main sources of Fe (Löscher et al., 1997; Croot et al., 2004; Grotti et al., 2005; Raiswell et al., 2006; Lannuzel et al., 2007, 2008; Tagliabue et al., 2010). The increase rate of glacial melt in West Antarctica during the last few decades, including the Pine Island Glacier (PIG) (Joughin et al., 2003; Rignot, 2008), implies an increased source of Fe in this region.

Antarctic coastal polynyas are areas of reduced sea ice cover within the ice pack and their associated surface waters are noted for enhanced levels of biological production during spring and summer (Arrigo and van Dijken, 2003; Arrigo et al., 2008a). Arrigo et al. (2008b) concluded that due to these high levels of biological production, in combination with high ventilation rates, formation of Antarctic Bottom Water and extensive winter sea ice cover, Antarctic shelf waters are a strong sink for anthropogenic CO_2 per unit area. The main controls on phytoplankton growth and primary productivity in polynyas are the availability of light and Fe (Arrigo et al., 2003), similar to open ocean regions in the Southern Ocean. In the Ross Sea polynya, the largest and most well studied polynya of the Antarctic, the availability of Fe controls the magnitude of annual primary productivity whereas light availability determines phytoplankton species distribution (Arrigo et al., 2000, 2003). A comprehensive satellite-based study of Antarctic coastal polynyas showed that although the Ross Sea polynya was the most productive, the polynyas of the Amundsen Sea and Pine Island Bay exhibited both the highest levels of phytoplankton biomass and the highest rates of primary productivity per unit surface area (Arrigo and van Dijken, 2003, Arrigo et al., 2012). Currently, it is not known what Fe sources fuel this intense and long-lasting phytoplankton bloom.

The Antarctic Circumpolar Current (ACC) is steered southward in the Pacific sector of the Southern Ocean due to fracture zones in the Pacific Antarctic Ridge. This causes the relatively warm Circumpolar Deep Water (CDW) to be positioned further south than in other regions of Antarctica. The southerly position of the CDW, in combination with a persistent clockwise-directed wind field, causes upwelling in the Amundsen Sea (Jacobs et al., 1996; Jacobs and Comiso, 1997; Hellmer, 2004). Cold shelf water is formed in winter and mixes with the incoming CDW during its descent down the continental slope. According to Assman and Timmermann (2005), the presence of the polynyas plays an important role in this mixing process because sea ice is constantly formed and blown away by the strong offshore winds that keep them ice-free. Brine expulsion during sea ice formation causes the cold water to become so dense that it sinks (Fichefet et al., 2003).

Pine Island Bay is affected by an increase in melting rate of floating glacier termini and surrounding ice shelves, most notable from the PIG, due to a change in the ocean heat transport beneath the glacier (Jenkins et al., 1997, 2010; Joughin et al., 2003; Rignot, 2008; Jacobs et al., 2011). Moreover, Jenkins et al. (2010) used an autonomous underwater vehicle to show that melting is also accelerating because of inland shifting of the grounding line of the glacier. The relatively warm CDW can thus flow over an underwater ridge and melt the bottom of the upstream part of the glacier.

The research presented here aims to identify and quantify the sources of Fe that fuel the phytoplankton blooms in the Pine Island Bay and Amundsen Sea polynyas. In particular, we quantified the input of Fe from the PIG into waters of Pine Island Bay and the Pine Island Polynya. To this end, concentrations of DFe and total dissolvable iron (TDFe) were measured in surface and subsurface waters (top 300 m) at these locations in January–February 2009.

2. Materials and methods

2.1. Cruise track and sampling strategy

The cruise NBP09-01 on the R.V.I.B. *Nathaniel B. Palmer* took place in January–February 2009 in the Amundsen Sea (Southern Ocean). The cruise track (Fig. 1) shows that the research focus was on sampling near the Pine Island Glacier (PIG). The 41 stations where water samples were taken for DFe analyses are indicated; at 20 of these stations, TDFe was also sampled (Fig. 1).

Temperature and salinity were measured with a Sea-Bird SBE 9/11+CTD mounted on a 24–10 L bottle SBE32 rosette. Temperature, conductivity, and dissolved oxygen were measured with dual sensor systems mounted vertically on a horizontal frame connected to the rosette frame near the bottom. Additionally, a single pressure Chelsea fluorometer and 25-cm WetLab transmissometer were attached to the rosette. Temperature and salinity have been transformed into conservative temperature (Θ in °C) and absolute salinity (S_A in g kg^{-1}) according to McDougall et al. (2009).

For trace metal clean sampling of the 41 profiles from the upper 300 m of the water column, modified GO-FLO samplers provided by the Royal NIOZ were attached to a non-metal wire using messengers to close the bottles. Sample depths were typically 10, 25, 50, 100, 200, and 300 m. Stations were chosen to encompass the diverse environmental conditions in the research area (Fig. 1). Open ocean, continental shelf, and glacier stations (especially PIG but also Getz, Crosson, and Dotson Ice Shelves) were sampled. On the shelf, sea ice covered stations and open water stations in the polynyas were sampled. In addition, surface water at eight stations (stations 5, 10, 37, 47, 94, 118, 129 and 135) was sampled and analyzed for DFe and TDFe. These samples were typically taken at 10 m depth to obtain large quantities of trace metal clean surface water for biological experiments.

Samples for DFe (filtered 0.2 μm pore size, Sartorius Sartobran-300) and TDFe (unfiltered) were taken directly from Teflon-coated GO-FLO bottles in a trace metal clean room. All sample bottles used for Fe analysis (Nalgene, Low-Density Polyethylene, LDPE, 60 to 1000 ml) were treated following GEOTRACES recommendations of a three-step cleaning procedure (detergent solution, 6 M HCl, and 3 M HNO_3) in a hot bath. Finally, the bottles were stored filled with 0.1 M 2QD-HNO_3 (distilled from 65% reagent grade, J.T. Baker). All rinsing was done with 18.2 MΩ cm^{-1} water (Millipore Milli-Q deionised water). Before sampling, the bottles were rinsed five times with about 20% of the sample bottle volume with the sample seawater.

2.2. Fe analysis

Samples for DFe analyses were filtered (0.2 μm), acidified (pH=1.8 by adding 2 ml per liter of ultraclean 12 M HClBaseline®Hydrochloric Acid, Seastar Chemicals), and measured directly on board by

Author's personal copy

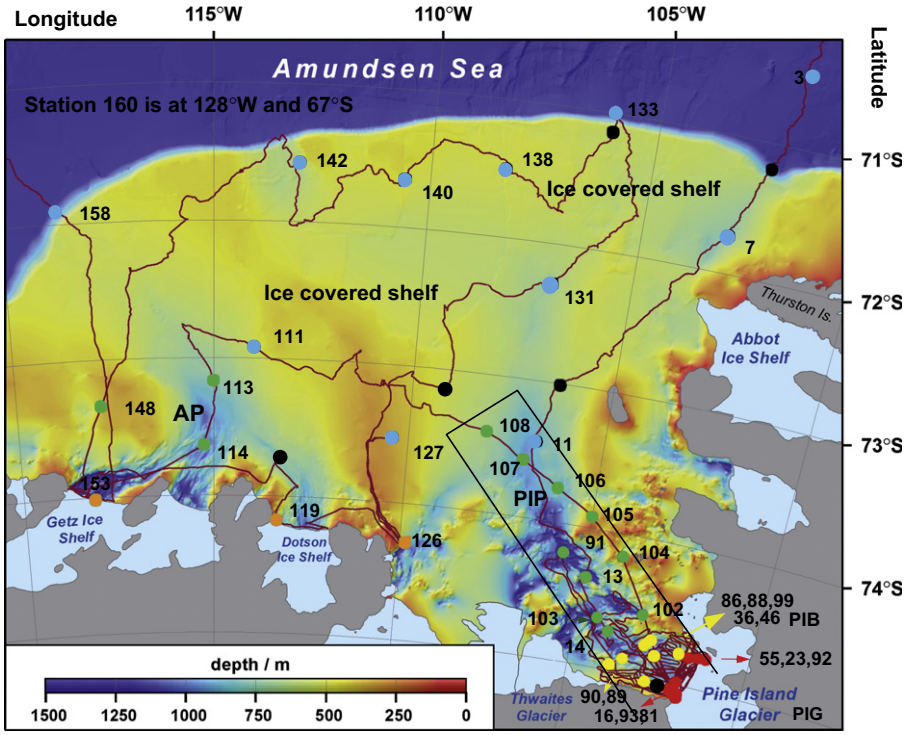

Fig. 1. Map of the research area where the top 300 m of the water column of 41 stations were sampled for Fe analyses. The different colors of the station numbers correspond to the different hydrographic environments. The rectangular section indicates the position of the section plots (Figs. 4 and 6). Black=open ocean station 160 (outside the map at 128°W and 167°S), blue=ice covered stations, green=polynyas—Pine Island Polynya (PIP) and Amundsen Polynya (AP), yellow=Pine Island Bay (PIB), red=adjacent to Pine Island Glacier (PIG), orange=adjacent to other glaciers (Dotson, Crosson and Getz ice shelf). Dots without station numbers represent stations where only surface waters were sampled (see Section 2).

automated Flow Injection Analysis (FIA) using the modified method of De Jong et al. (1998) as described in De Baar et al. (2008a).

Samples were analyzed in duplicate sample bottles, each of which was measured in triplicate (for a total of six analyses per sample). Mean DFe concentrations and standard deviations are given. Concentrations of measured DFe ranged from 0.03–1.31 nM. The blank was measured daily during the entire cruise and had a mean value of 0.023 ± 0.010 nM ($n=39$), defined as a sample loaded for 10 s. The Fe added by the Seastar acid (at maximum ~0.4 pM) was neglected. The average limit of detection (0.009 ± 0.008 nM) was defined as being three times the standard deviation of the daily mean blank ($n=3$).

The consistency of the FIA system over the course of the day was verified using a drift standard (same sample measured three or four times throughout the day). The drift was observed to be less than 7% and no corrections have been made for this drift. Accuracy and reproducibility were checked by regularly measuring two SAFe reference standard samples. The results (S1: 0.078 ± 0.012 nM DFe, $n=10$ and D2: 0.942 ± 0.043 nM, $n=13$) were well within the community consensus values (S1: 0.097 ± 0.043 nM DFe, $n=140$ and D2: 0.91 ± 0.17 nM, $n=168$, Johnson et al., 2007).

In addition, unfiltered samples (19 profiles and 8 surface stations) were acidified to pH=1.8 and stored. The TDFe concentration of each sample was measured (as described above for DFe) at the NIOZ home laboratory after at least six months.

The Fe data can be found on the GEOTRACES website: http://www.bodc.ac.uk/geotraces/. At the time of publication of this paper, the website did not yet contain the data, therefore, the following website was constructed to make the data available: http://www.nioz.nl/public/ipy/polardata.php?crsid=181.

2.3. Chlorophyll a analysis

Chlorophyll *a* (Chl *a*) concentrations were measured using standard JGOFS procedures (JGOFS, 1996). Chl *a* samples (0.05–1 L) were filtered onto 25 mm GF/F filters (Whatman, nominal pore size 0.8 μm) at ambient seawater temperature under low vacuum pressure. Filters were extracted in 5 ml of 90% acetone in the dark at 4 °C for 20 h. The extracted fluorescence was determined before and after acidification using a Turner Designs Model 10-AU fluorometer.

2.4. Vertical eddy diffusivity estimates using CTD-data

Vertical turbulent eddy diffusivity (K_z) was estimated by calculating the Thorpe scale using 1-m binned CTD data. The Thorpe scale is a vertical length scale of turbulent mixing in a stratified flow (Thorpe, 1977). It is obtained after rearranging an observed potential density profile, which may contain inversions associated with turbulent overturns, into a stable profile without inversions. The method of overturn displacements provides a reasonably adequate estimate of vertical turbulent eddy diffusivity and dissipation rate to within a factor of two, as has been established after comparison with free-falling microstructure data (e.g., Hosegood et al., 2005).

The vertical displacement necessary for generating the stable profile is the Thorpe displacement. Then, defining d_T as the root mean square of the Thorpe displacements within each overturn, the eddy diffusivity ($m^2\ s^{-1}$) is defined as,

$$K_z = 0.128 d_T^2 N \quad (1)$$

where N denotes the buoyancy frequency and the constant 0.128 was derived from an empirical relation with the Ozmidov scale

Author's personal copy

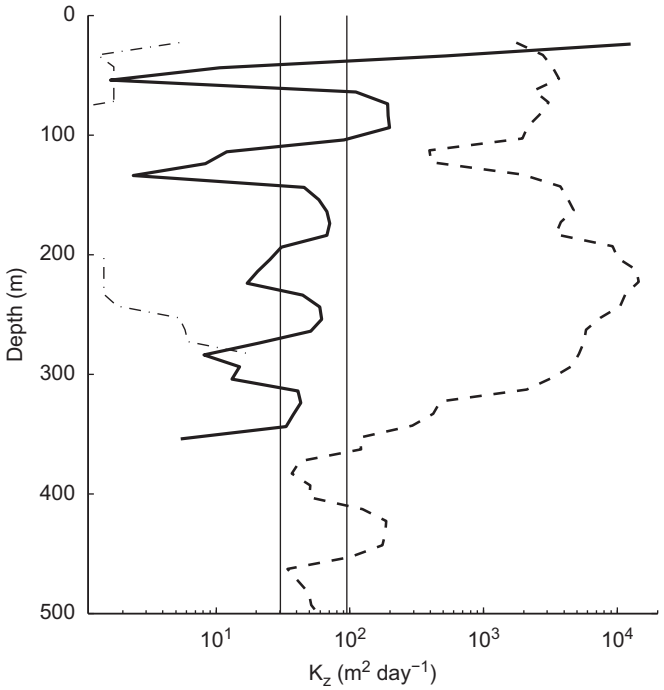

Fig. 2. Vertical turbulent eddy diffusivity (K_z) profiles averaged in 30 m vertical bins for stations 16 (thick dashed line), 102 (solid line), and 105 (thin dashed line). The vertical lines indicate the K_z values from Park et al. (2008) and Planquette et al. (2007) of 27.6 and 95 $m^2\,d^{-1}$ (3.2×10^{-4} $m^2\,s^{-1}$ and 11×10^{-4} $m^2\,s^{-1}$), respectively.

using a mixing efficiency of 0.2 (Dillon, 1982). The raw $K_z(z)$ profile is averaged in 30-m vertical bins (Fig. 2), which is equivalent to the largest displacement observed. Subsequently, a mean value per station is obtained for the depth-range between 100 and 300 m to within a standard error of a factor of two (Table 1).

3. Results

3.1. Hydrography

Five different hydrographic environments in the Amundsen Sea were identified from typical property–property plots of conservative temperature (Θ) and salinity (S) (Fig. 3A,B and C). These include (1) open ocean (st 160), (2) ice covered regions close to and on the continental shelf (st 3, 7, 11, 111, 127, 131, 133, 138, 140, 142 and 158), (3) the Pine Island Polynya (PIP) (st 13, 14, 91, 102, 103, 104, 105, 106, 107 and 108) and the Amundsen Polynya (AP) (st 113, 114 and 148), (4) Pine Island Bay (PIB), located 10–60 km from the PIG (st 36, 46, 86, 88, 89, 90 and 99) where waters were free of ice and surface concentrations of Chl *a* were lower than those of the PIP, and (5) glacier stations that were influenced by both upwelling and glacial melting and were located within 10 km of a glacier. Glacier stations were located predominantly near the PIG (st 16, 23, 55, 81, 92 and 93) but also near the Dotson, Crosson, and Getz Ice Shelves (st 119, 126 and 153, respectively) (Figs. 1, 3A and 3D).

At open ocean st 160, CDW (defined as $\Theta=\leq2$ °C and S_A=34.2–34.7 g kg^{-1}, Giulivi and Jacobs, 1997) is present below 200 m (Fig. 3B). Winter water (WW, defined as $\Theta=-1.5$ °C and S_A=34.2 g kg^{-1}), which is cold water formed during the previous winter, is present between 100 and 150 m.

At ice covered st 3 located just off the shelf, modified CDW (MCDW) with a lower temperature ($\Theta=-1.6$ to 1.7 °C; S_A=34.3–34.7 g kg^{-1}) was overlying the CDW. At st 133 and 158 near the continental shelf break (Fig. 1), deep water (300 m) consisted primarily of MCDW. These stations had lower surface temperatures ($\Theta=-1.7$ °C) and no distinct WW layer. The relatively low salinities (S_A=33.2–33.7 g kg^{-1}) near the surface indicated the melting of surrounding sea ice. The ice covered stations located on the shelf shared similar vertical Θ and S_A profiles (as shown in Fig. 3B) and similar property–property plots (nutrient concentrations, Alderkamp et al., 2012). Towards the polynya, the nutrient concentrations gradually decreased, surface temperatures increased up to 0–0.5 °C, and a WW layer could be distinguished.

Plots of Θ–S_A for PIP stations 102, 103 and 106 (Fig. 3C) suggested the presence of MCDW below 200 m, similar to the ice covered stations. A temperature minimum was apparent above the MCDW, indicative of a pronounced WW layer between 100 and 150 m (Figs. 3C and 4A). Within the PIP, there were pronounced surface temperature differences between stations, even at polynya stations in close proximity of each other. For example, the near-surface Θ–S_A plot for st 102 indicates recent mixing (Fig. 3C), which is evidenced by the counter density gradient loops shown in the inset in Fig. 3D, whereas stations 104 (not shown) and 106 show Θ–S_A plots of a stable water column.

PIB stations were located between stations within the PIP and stations that were strongly influenced by the glacier. They have relatively high surface temperatures but were distinct from the PIP stations because they exhibited lower surface Chl *a* concentrations (Alderkamp et al., 2012). As expected, the Θ–S_A plot from st 86 in the PIB shows intermediate temperatures and salinities compared to those of PIP and PIG stations (Fig. 3A).

The difference in Θ–S_A plots between st 16 and 55 near the PIG, st 119 near the Dotson Glacier, and st 153 near the Getz Ice Shelf reflects the different processes in these hydrographic environments (Fig. 3D). The upwelling MCDW exhibited relatively high temperatures and salinity (Θ=0–1 °C; S_A=34.5–34.8 g kg^{-1})

Table 1
The vertical turbulent eddy diffusivity K_z of selected stations as a mean value between 100 and 300 m. Pine Island Polynya (PIP), Amundsen Polynya (AP), Pine Island Bay (PIB).

Environment	Station	K_z ($m^2\,d^{-1}$)
Ice covered shelf	140	0.4
Ice covered shelf	142	0.4
Ice covered shelf	158	1.5
	Mean ice covered shelf	***0.8 ± 0.6***
PIP	13	25.1
PIP	14	6.4
PIP	91	207.4
PIP	102	33.7
PIP	103	6.2
PIP	104	293.8
PIP	105	2.7
PIP	106	4.4
PIP	107	16.4
PIP	108	25.9
	Mean PIP st 91 and 104	***250.6 ± 61.1***
	Mean PIP others	***14.7 ± 11.9***
	Overall mean PIP	***62.2 ± 101.9***
AP	113	5.3
AP	114	6.6
AP	148	3
	Mean of Amundsen polynya	***4.9 ± 1.8***
PIB	86	25.1
PIB	88	8.6
PIB	99	0.6
	Mean PIB	***11.2 ± 12.5***
PIG	16	6134.4
PIG	55	62.2
	Mean PIG	***3110 ± 4293***
Dotson Glacier	119	81.2
Getz glacier	153	129.6
	Mean of other glaciers	***103.7 ± 34.2***

Author's personal copy

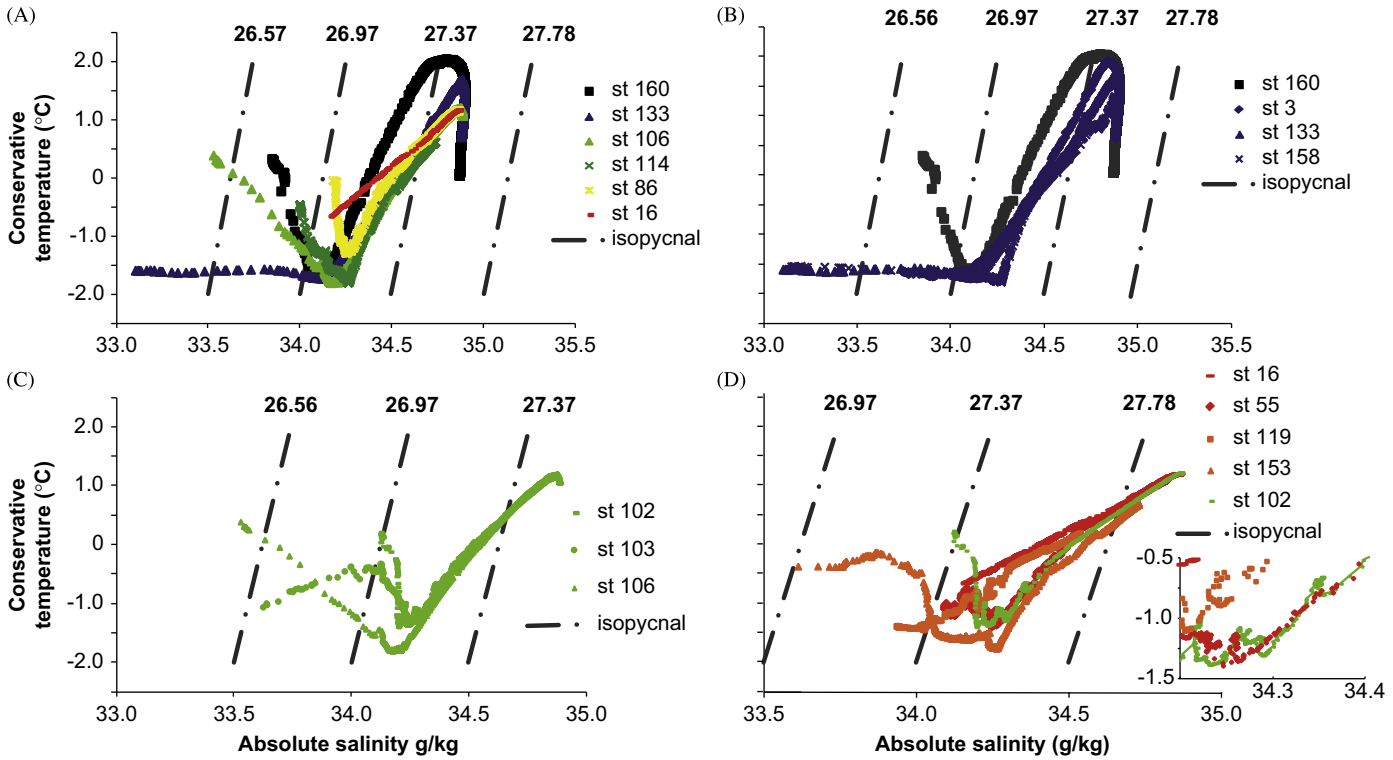

Fig. 3. Conservative temperature (Θ in °C) versus absolute salinity (S in g kg^{-1}) plots of selected stations. The dashed lines indicate isopycnals, lines of constant potential density, whose values are indicated on top of the isopycnals (kg m^{-3}). The selected stations represent the different hydrographic environments of the Amundsen Sea, including open ocean (black), sea ice zone (blue), polynyas (light green for the PIP, dark green for AP, yellow for PIB), and near glaciers (red for PIG and orange for the Dotson, Crosson and Getz Ice Shelves). (A) Examples from each of the different hydrographic environments. (B) Both open ocean (st 160) and ice covered stations (st 3, 133, and 158). The modification of the CDW in ice covered stations is apparent by comparing station 160 with the others. (C) Three stations from the central PIP. (D) examples of stations near the PIG (red) and other glaciers (orange). Station 102 (green) from the central PIP is added. In the enlarged inset, counter density gradient loops are shown as evidence of recent mixing.

below 300 m depth (Fig. 3A and D). At the surface, the effect of dilution by glacier meltwater was apparent by its lower salinity ($S_A \leq 34.2$ g kg^{-1}) compared with MCDW and a lower surface temperature than in the PIG. Station 16 (located at the southern end of the PIG) and st 119 (located at the western end of the Dotson Ice Shelf) exhibited evidence of vigorous vertical mixing, resulting in nearly straight Θ–S-plots. Such a linear relationship could also represent near-coastal new water mass formation above a frontal zone and subsequent isopycnal transport into the interior, but the overturn of the individual $\Theta(z)$ and $S(z)$ profiles support the presence of local mixing. On the other hand, st 55 (located at the northern end of the PIG) contained a distinct WW layer, indicating some stratification. Station 153 near the Getz Ice Shelf even showed two temperature minima, a broad minimum ($\Theta = -1.55$ °C) at 130 m and a narrow minimum ($\Theta = -1.7$ °C) at 347 m, and had more saline waters than the other glacier stations below the minima (Fig. 3C). The presence of cold water at 347 m reflected the absence of upwelling MCDW in this location.

Vertical sections along a transect from the PIG to the PIP (Fig. 4A,B and C) showed distinct changes in temperature, salinity, and Chl *a* with increasing distance from the glacier. Since there was large temporal variation in sampling during NBP09-01, the sequence between st 81 (sampled on 25 January) and st 108 (sampled on 1 February) was chosen for the vertical sections because they represent the same stage of the phytoplankton bloom in the polynya.

Surface Chl *a* concentrations (Fig. 4C) were high (up to 15 μg l^{-1}) in the PIP, whereas nutrient concentrations were low ($NO_3+NO_2 <$ 5 μM; Alderkamp et al., 2012). At depth, nutrient concentrations in the polynya were high (NO_3+NO_2 near 30 μM, Alderkamp et al., 2012) in both the WW layer and the MCDW. In the upwelling MCDW in front of the PIG, concentrations of NO_3+NO_2 were similarly high, whereas phytoplankton were virtually absent.

3.2. Fe concentrations

Concentrations of DFe and TDFe are shown in vertical profiles grouped by their hydrographic location (Fig. 5) as well as in section plots from the PIP to the PIG (Fig. 6A and B). Because fewer stations were sampled for TDFe, the section plot of TDFe data was expanded to include all stations in the transect zone instead of only stations sampled between 25 January and 1 February, as in Figs. 4A,B and C and 6A.

3.2.1. Open ocean

At st 160, Fe concentrations were generally low (0.03–0.23 nM DFe and 0.31–4.31 nM TDFe (Fig. 5). Dissolved Fe showed a typical nutrient-type profile, being lowest (0.03 nM) near the surface and higher (0.16 nM) at 300 m. In contrast to DFe, TDFe concentrations were relatively high near the surface (2.04 nM at 10 m).

3.2.2. Ice covered shelf stations

Station 7 showed an exceptionally high surface concentration of 0.40 nM DFe above a steep decrease to a subsurface minimum of 0.08 nM DFe at 25 m. It is possible that melting of the Abbot Ice Shelf contributed to this elevated DFe concentration relative to other ice covered stations. Stations 111, 127, 140 and 142, situated between 110°W and 115°W, did not exhibit a surface maximum in DFe.

Author's personal copy

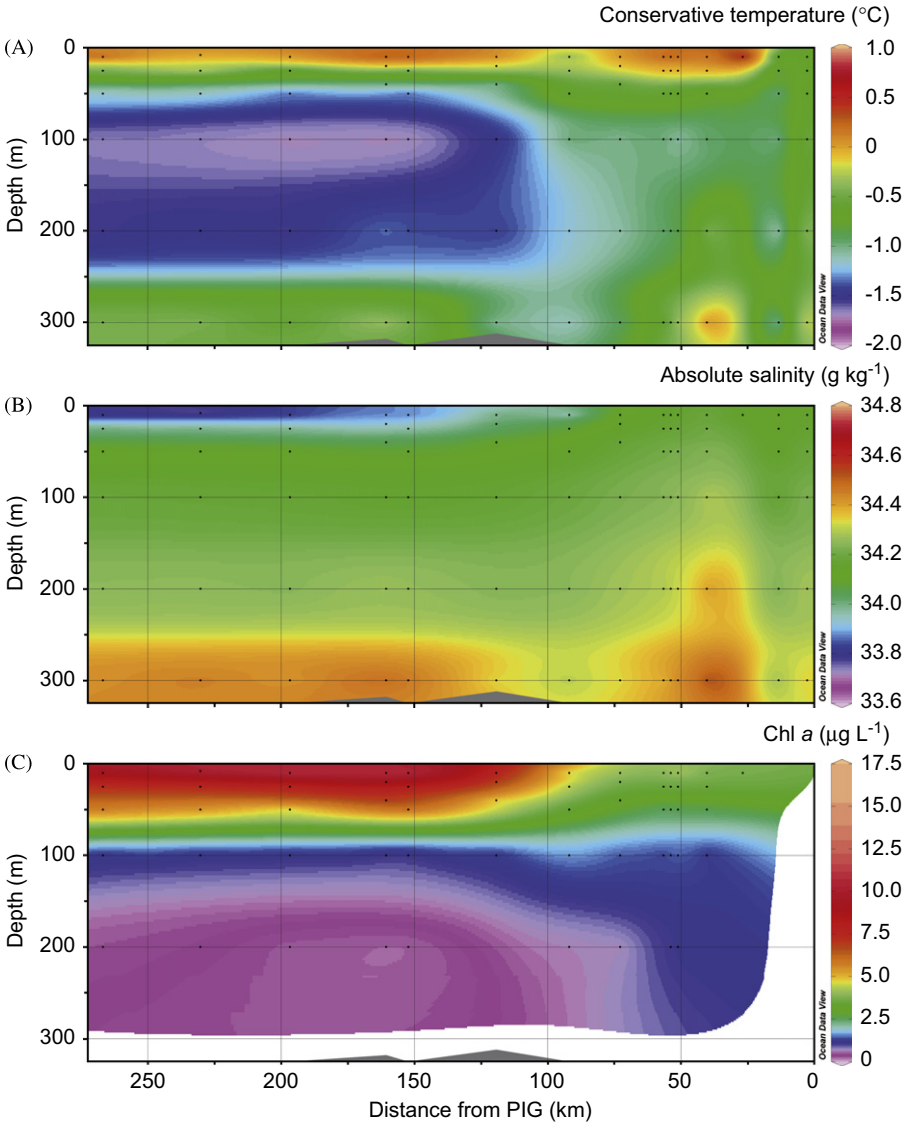

Fig. 4. Water properties along a transect northwestward from the PIG tongue, via Pine Island Bay into the Pine Island Polynya (see Fig. 1 for the position of the section), including (A) conservative temperature (°C), (B) absolute salinity (g kg^{-1}), and (C) chlorophyll *a* (µg l^{-1}). Horizontal distance is in km from the PIG. Only stations sampled between 25 January and 1 February (stations 81–108) were included.

TDFe exhibited similar profiles, with constant concentrations at st 131–142 (Fig. 5). However, st 158 on the continental shelf edge had high TDFe concentrations below 100 m of 10–23 nM. Sediment along the continental margin is probably the Fe source here. On the shelf edge, turbulence caused by down slope currents may resuspend sediment particles and thus increase TDFe concentrations. This is supported by the mean vertical turbulent eddy diffusivity of 1.5 $m^2\,d^{-1}$ in the upper 500 m at st 158. This diffusivity is 3.6 times that of nearby stations 140 and 142 which are further south from the continental shelf edge (Fig. 1, Table 1).

3.2.3. *Pine Island Polynya*

The lowest DFe concentrations (0.04 to 0.07 nM) were measured in subsurface waters (25–50 m) at st 13, 14, 91, and 102–108, below a small surface maximum of 0.07–0.17 nM DFe at 10 m. Deeper in the water column (300 m), DFe concentrations increased to 0.25–0.61 nM (Figs. 5 and 6). DFe concentrations were highest at 300 m at both st 13, with a depth of 1294 m, and at st 105, where the depth was only 318 m. Although a flux of Fe from the sediment may have increased deep DFe concentrations at st 105, this cannot be the only explanation for its elevated DFe concentrations. The bottom depth of neighboring st 104 was similar to that of st 105, yet the DFe concentrations at 300 m at this station were lower and resembled those of the deep st 91 (1028 m depth).

TDFe profiles in the PIP were similar for st 104–108, with relatively constant TDFe concentrations in the upper 100 m of 1.4–5.9 nM, increasing to 8–12 nM at 300 m. Station 102 showed remarkably high TDFe concentrations, resembling those of glacier st 16 in front of the PIG. Variations in temperature with depth were also observed in st 102, and the density profile indicates a stable water column (Fig. 3C and D). However, recent mixing at this station is suggested by a relatively high K_z of 33.7 $m^2\,d^{-1}$ (2.2 times higher than the mean in the PIP, with the exception of the substantially higher K_z at st 91 and 104) (Fig. 2 and Table 1). A recent passage of a melting iceberg could explain the variations in temperature and salinity as well as the elevated TDFe concentrations (Stephenson et al., 2011; Raiswell, 2011; Lin et al., 2011).

Author's personal copy

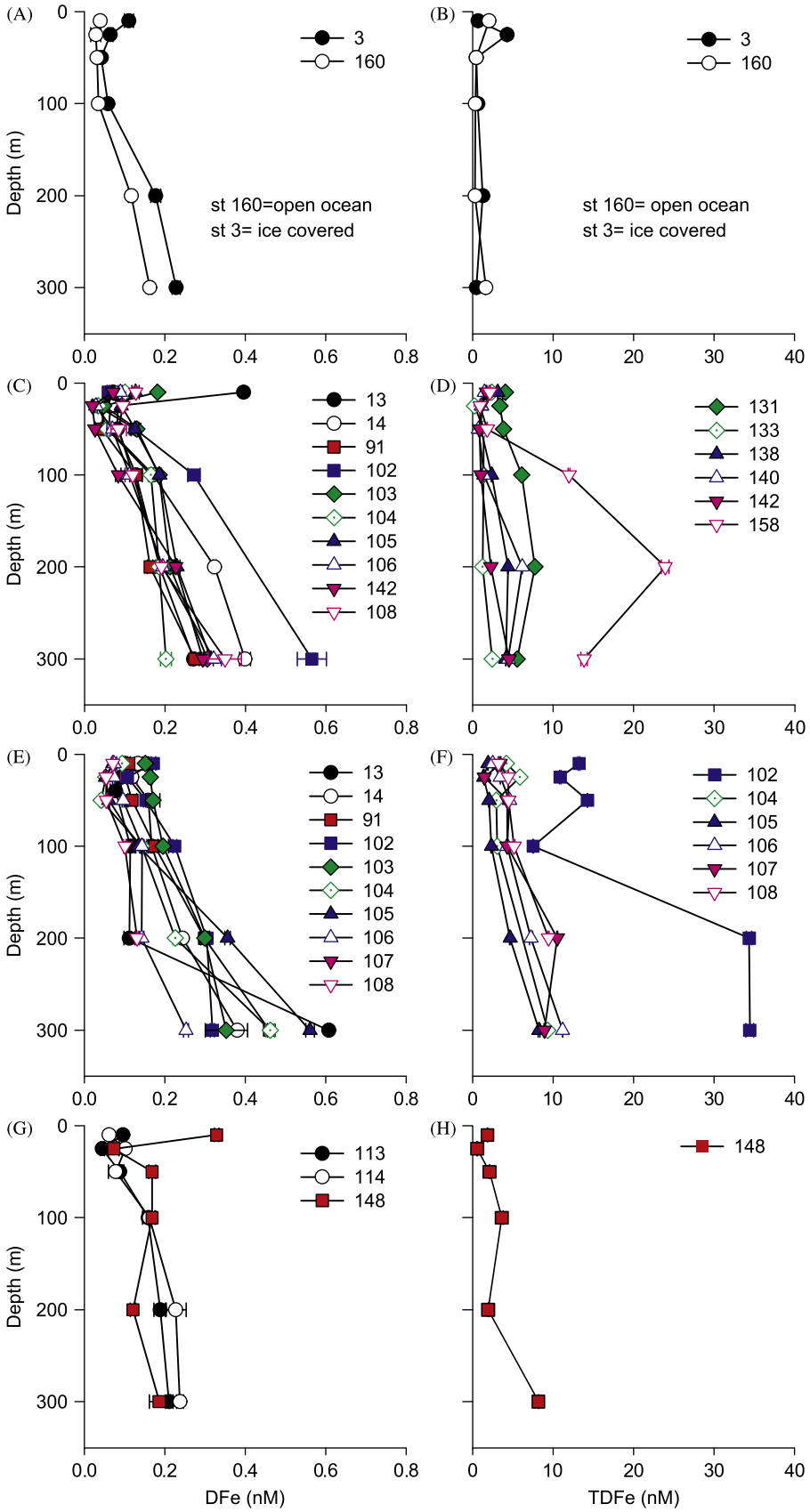

Fig. 5. Concentrations of dissolved Fe (DFe) (left) and total dissolvable Fe (TDFe) (right) with depth for different hydrographic environments. Error bars represent the STD of 6 measurements. Note the difference scales in DFe and TDFe concentrations of the glaciers stations. (A) DFe concentrations in open ocean station 160 and ice covered station 3, (B) TDFe concentrations in open ocean station 160 and ice covered station 3, (C) DFe concentrations in ice covered stations other than station 3, (D) TDFe concentrations in ice covered stations, (E) DFe concentrations in PIP stations, (F) TDFe concentrations in PIP stations, (G) DFe concentrations in AP stations, (H) TDFe concentrations in AP stations, (I) DFe concentrations in PIB stations, (J) DFe concentrations in PIG stations, (K) TDFe concentrations in PIG stations, (L) DFe concentrations stations near the Dotson, Crosson and Getz Ice Shelves, (M) TDFe concentrations in stations near the Dotson, Crosson and Getz Ice Shelves.

Author's personal copy

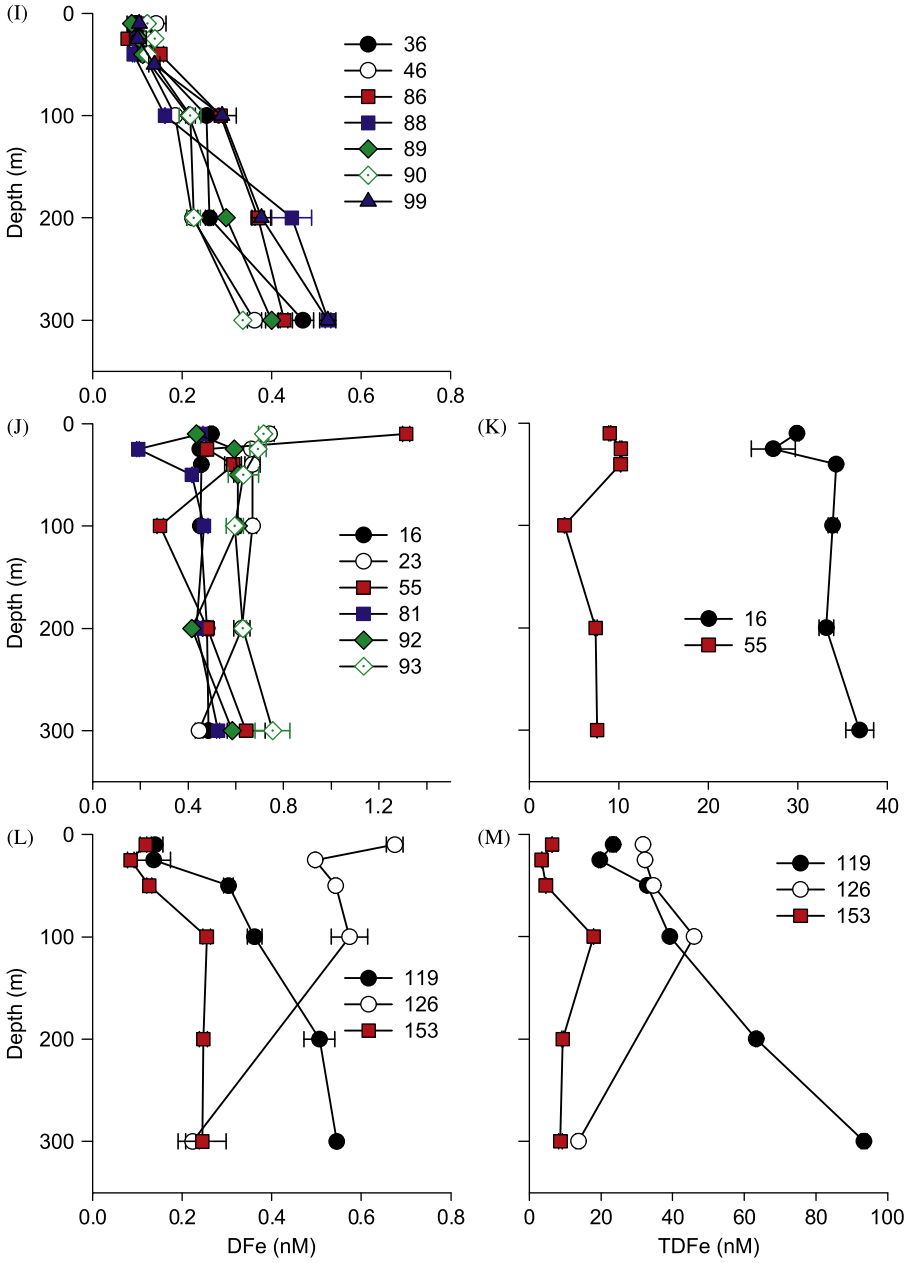

Fig. 5. (*continued*)

3.2.4. *Amundsen Polynya*

DFe concentrations in the upper 200 m of the AP at st 113, 114, and 148 were similar to those in the PIP (Fig. 5). However, they differed from most PIP stations by their relatively low DFe concentrations at 300 m ($\leq$ 0.3 nM), suggesting perhaps that the MDCW is less modified in the AP (Fig. 3A). Although water depths in the AP were comparable to those in the PIP, there was no apparent influx of DFe from the sediment (depths were 763, 923, and 365 m for st 113, 114, and 148, respectively).

The single TDFe profile from the AP (st 148) was similar to those from the PIP (Fig. 5), ranging from 0.6–2.1 nM in the upper 50 m to 8.2 nM at 300 m.

3.2.5. *Pine Island Bay*

Stations in PIB exhibited surface DFe concentrations between 0.08 and 0.14 nM, slightly higher than those of the PIP. These concentrations increased to 0.3–0.5 nM at 300 m with no apparent subsurface minimum.

While no TDFe profiles are available from PIB, surface TDFe concentrations averaged 7.9 ± 1.2 nM for the three stations sampled.

3.2.6. *Pine Island Glacier and other glacier stations*

The stations adjacent to the PIG and the Crosson, Dotson, and Getz Ice Shelves exhibited the highest DFe concentrations of the entire study region (0.4–0.8 nM near the PIG and 0.2–0.6 nM near the ice shelves in the Amundsen Sea). The DFe concentrations were relatively constant with depth (Figs. 5 and 6) at stations influenced by upwelling under the glaciers and subsequent mixing, as indicated by the Θ–S plots (Fig. 3). Only st 153, located close to the Getz Ice Shelf, showed a DFe profile similar to those observed elsewhere in the area, with low concentrations near the surface ($<$ 20 m; 0.09 nM) and increasing with depth (0.24 nM).

Author's personal copy

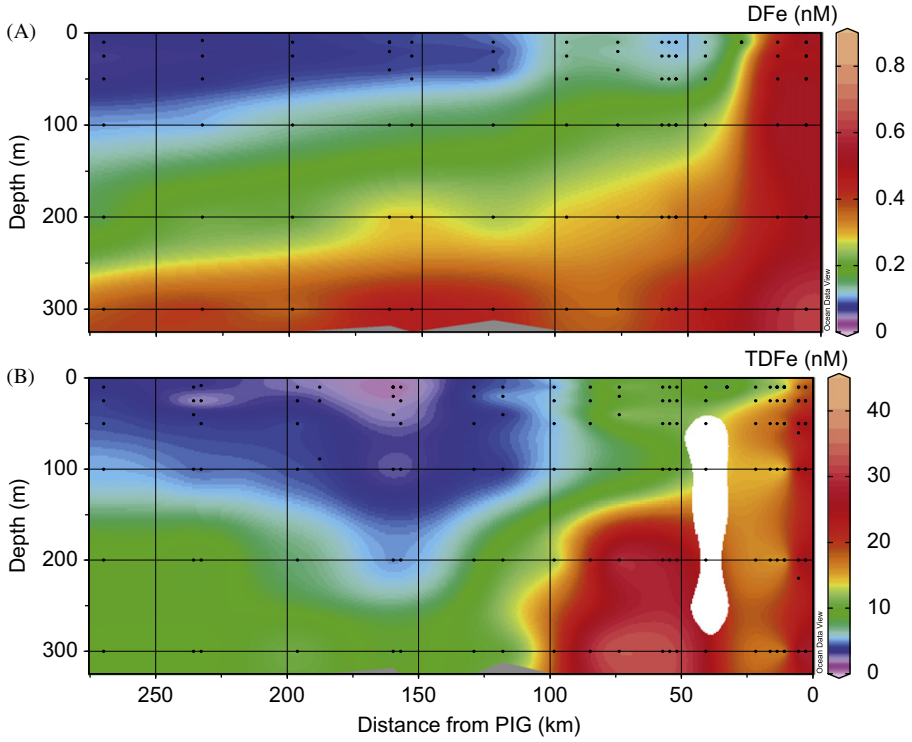

Fig. 6. Vertical sections of dissolved Fe (DFe) (A) and total dissolvable Fe (TDFe) (B) along a transect northwestward from the PIG tongue, via Pine Island Bay into the Pine Island Polynya (see Fig. 1 for the position of the section). The stations shown in (A) are similar to those shown in Fig. 4, in (B) also data from station 16 and 55 were used.

This station exhibited evidence of stratification (observed from the Θ–S plots), suggesting a reduction in the rate of upwelling and mixing with meltwater that characterized the other glacier stations (Fig. 3D), as described by Jacobs et al. (2011).

The TDFe concentrations of glacier stations exhibited considerable spatial variation (Fig. 5), with st 16 on the southern end of the PIG having an average concentration of 32.6 nM and st 55 on the northern end of the PIG having an average concentration of 8.1 nM. Station 126, located close to the Crosson Ice Shelf, had a subsurface maximum TDFe concentration of 43 nM at 100 m, which declined to 31 nM near the surface and to 14 nM at 300 m. TDFe concentrations at st 119, located near the Dotson Ice Shelf, were approximately 25 nM near the surface but increased to 106 nM at 300 m, the highest concentration measured in this study. In contrast, st 153 had the lowest TDFe concentrations of all glacier sites, resembling those of the AP stations.

4. Discussion

4.1. Fe distributions

4.1.1. DFe

Low DFe concentrations, due to the lack of Fe sources, were measured in the open ocean station, resembling those reported in previous publications from the Southern Ocean (Measures and Vink, 2001; De Baar and De Jong, 2001; Croot et al., 2004, Sedwick et al., 2008; Klunder et al., 2011). DFe concentrations were low in the subsurface (25–50 m depth) in almost all environments except in the glacier stations (Figs. 5 and 6A). The lowest subsurface DFe concentrations (0.04–0.1 nM) were found in the PIP and the AP associated with high phytoplankton biomass (up to 13.9 and 3–5 $\mu g\,l^{-1}$ Chl a, respectively, Alderkamp et al., 2012), suggesting that these low DFe concentrations were driven by the uptake by phytoplankton (De Baar and De Jong, 2001; Measures et al., 2008; Klunder et al., 2011). Higher surface (10 m depth) DFe concentrations indicate input from melting sea ice in the ice covered, polynya, and near glacier stations, as has been seen in other Antarctic environments (Sedwick et al., 2000; Measures and Vink, 2001; Lannuzel et al., 2008).

The increase in DFe between 100 and 300 m between the open ocean and the glaciers coincides with the presence of MCDW. Near the glaciers, DFe concentrations were relatively high and spatially and temporally heterogeneous due to the different rates of upwelling and subsequent mixing with the glacier melt water (Jacobs et al., 2011; Fig. 5). At stations with a tight linear Θ–S relationship over the entire depth (suggesting vigorous vertical mixing), the DFe concentrations were considerably higher (st 16 in front of the PIG see also Fig. 3D) than at stations with less mixing (low DFe concentrations at st 153 in front of the Getz Ice Shelf, Fig. 3D).

The concentrations of DFe in the glacier stations were generally in the range of 0.4–0.8 nM DFe, reaching 1.31 nM in the surface layer at st 55. Thuróczy et al. (2012) found that dissolved organic ligands were nearly saturated with Fe near the PIG. Saturation of the ligands is an indication that the DFe concentrations we observed were likely to be maximum values beyond which DFe would precipitate.

4.1.2. TDFe

'As shown for DFe, TDFe concentrations at 100–300 m increased between the open ocean and the glaciers (Fig. 5). At this depth, TDFe concentrations in the PIP were relatively high with a large standard deviation (TDFe$=10.3\pm10$ nM, $n=16$). Excluding the anomalously high values at st 102 reduces the mean and standard deviation to 6.8 ± 3 nM ($n=13$),comparable to concentrations observed in the Ross Sea (Sedwick et al., 2000). The concentrations near the glaciers were extremely high, but also highly variable ([TDFe]$=20.3\pm13.1$ nM, $n=12$; [TDFe]$=28.3\pm23.5$ nM, $n=17$, respectively). At the surface, meltwater MDCW (meltwater-enriched MDCW) advects northward in well-defined cores of outflow, separated by depth and

Author's personal copy

location along the ice front (Mankoff et al., 2012). The presence of such outflows explains the large variation in surface TDFe concentration at glacier stations (3–93 nM) as well as the variability in other parameters like DFe (0.2–1.3 nM), salinity (34.09–34.37 g kg^{-1}), and temperature (−0.1–1.7 °C, see also Figs. 4–6). The high turbulence of the waters at st 16 and 119 are shown by the Θ–S plots (Fig. 3D) and by the high K_z values near the glaciers (up to 6134 m^2 d^{-1}; Table 1). It can be concluded that upwelling of MCDW and mixing with meltwater were the primary processes producing high TDFe concentrations near the glaciers (Fig. 5).

4.2. Fe budget

4.2.1. Phytoplankton uptake

The phytoplankton blooms in the polynyas were dominated by the haptophyte *Phaeocystis antarctica*, whereas the phytoplankton community in ice covered stations was a mix of diatoms and *Phaeocystis antarctica* (Alderkamp et al., 2012). According to satellite observations, the phytoplankton bloom in the PIP during the course of our study started on 12 December 2008 and lasted for 73 d (Arrigo et al., 2012). When Fe addition bioassay experiments were performed on 30 January 2009 and 6 February 2009, no Fe-limitation of phytoplankton growth was observed (Mills et al., 2012). Therefore, this bloom must have had access to an adequate supply of bioavailable Fe. By calculating how much Fe was needed to sustain the observed bloom, we can evaluate the relative contribution of Fe by the different possible Fe sources.

We calculated the total Fe requirement by the *P. antarctica* bloom in the PIP by calculating the Fe requirement of the phytoplankton biomass. Phytoplankton biomass in the upper mixed layer was approximated by measurements of the mean satellite derived Chl *a* concentration in the PIP (2.09 mg Chl *a* m^{-3}; Arrigo et al., 2012), the phytoplankton C:Chl *a* ratio (100 g g^{-1}) (Thompson et al., 1992), and the Fe:C ratio for *P. antarctica* single cells and colonies (23.4 and 93.4 μmol mol^{-1}, respectively, Schoemann et al., 2001, 2005; Hassler and Schoemann, 2009). This calculation (mg Chl *a* m^{-3} × mg C: mg Chl *a* × mmol C: 12 mg C × nmol Fe: mmol C = nmol Fe) yields a total Fe requirement by the *P. antarctica* bloom of 0.4–1.6 nM TDFe, depending on the Fe:C ratio used. Fe:C ratios of phytoplankton in the literature range from 0.8 to 93.4 μmol mol^{-1} (De Baar et al., 2008b; Hassler and Schoemann, 2009; Strzepek et al., 2011). According to Twining et al. (2004), the variation in Fe:C ratios can be attributed to differences in plankton community composition, ambient Fe concentration, incident irradiance, and other environmental parameters. The discrepancies may also be the result of methodological differences, including the use of different algorithms in the calculations (Strzepek et al., 2011). Here we choose to use the Fe:C ratios from Schoemann et al. (2001) and Hassler and Schoemann (2009) since they focused on *Phaeocystis*. The Fe:C ratios of 31–37 μmol mol^{-1} estimated by Twining et al. (2004) for natural phytoplankton populations under Fe replete conditions after Fe enrichment during SOFEX, fall within the range of Fe:C used here for *P. antarctica*.

According to data from Alderkamp et al. (2012), phytoplankton growth rates in the PIP in the upper mixed layer (15.2 m) were 0.37 ± 0.081 d^{-1}, in close agreement of the growth rates presented for *P. antarctica* in the Ross Sea by Smith et al. (1998). Given this growth rate, the flux of Fe to the upper mixed layer of the PIP (mean 15.2 m) necessary to sustain the observed phytoplankton bloom would have been 2.3–9.1 × 10^{-6} mol Fe d^{-1} (0.4–1.6 × 10^{-9} mol TDFe L^{-1} × 1000 = mol m^{-3} × 15.2 m = mol m^{-2} × 0.37 = mol m^{-2} d^{-1}).

Another approach to estimate the Fe requirement of the bloom is to use the new production rate, estimated to be 1.26 g C m^{-2} d^{-1} based on NO_3 removal between 12 December and the time of sampling (Alderkamp et al., 2012; Arrigo et al., 2012). Assuming that 97% of the primary production occurs in the upper mixed layer (Alderkamp et al., 2012) and using the same range for the Fe/C ratio (23.4–93.4 μmol mol^{-1}), a new production rate of 1.26 g C m^{-2} d^{-1} yields a similar Fe demand as obtained with the biomass calculation above of 2.4–9.5 × 10^{-6} mol Fe m^{-2} d^{-1} (PP × 0.97 g C m^{-2} d^{-1}/12 g C/mol C × mol Fe: mol C = mol Fe m^{-2} d^{-1}) (Table 2).

Can the Fe demand of 2.4–12.4 × 10^{-6} mol Fe m^{-2} d^{-1} by the *P. antarctica* bloom be supplied by the available Fe sources? Before the individual Fe sources are discussed, some points need to be addressed. It must be noted that regeneration is not taken into account and could contribute up to 50% of Fe demand (Sarthou et al., 2008). In addition, the winter stock of Fe is discarded as a Fe source because it is insignificant. This is because at the start of the bloom, the winter stock of DFe in the WW of the PIP would have been 0.19 ± 0.08 nM (n = 20). At the time of our study, DFe at 25 m had been reduced to 0.09 nM, indicating that phytoplankton had consumed 0.1 nM of the winter stock of DFe during the first 50 d of the bloom (between 12 December, the start of the bloom according to Arrigo et al., 2012, and 31 January, the sampling date of the PIP). The deficient of 0.1 nM DFe in the upper 15.2 m after 50 d results in a flux of only 3.0 10^{-8} mol DFe m^{-2} d^{-1}, which amounts to < 1% of the demand. This strongly suggests that an additional source of Fe was fueling the phytoplankton blooms.

The potential external Fe sources are (1) upwelling of CDW, (2) vertical diffusion from the sediments and subsequent diffusive or advective transport (Blain et al., 2007, 2008; Planquette et al., 2007), (3) dust input (Edwards and Sedwick, 2001; Edwards et al.,

Table 2
Fluxes of dissolved Fe (DFe) and total dissolvable Fe (TDFe) to the phytoplankton bloom in the PIP. See text for details for estimating the sink flux of Fe due to phytoplankton uptake. The fluxes from upwelling, vertical diffusion are maximum estimates. The distances of 40, 70 and 159 km from the PIG correspond to stations 99, 102 and 105, respectively. TDFe fluxes are approximate and presented in italic, since assumptions made are valid only for dissolved species.

Sources and sinks	Flux DFe (mol m^{-2} d^{-1})	Flux TDFe (mol m^{-2} d^{-1})
Sink by phytoplankton uptake		
By TDFe: biomass ratios	2.3 × 10^{-6}–9.1 × 10^{-6}	
By primary production	2.4 × 10^{-6}–9.5 × 10^{-6}	
Sources		
Upwelling	4 × 10^{-8}	*twice DFe?*
Vert. diffusion	9 × 10^{-8}	*2.2 × 10^{-6}*
Dust	3 × 10^{-10}	*3 × 10^{-9}*
Sea ice melt	6.8 × 10^{-8}	*1.9 × 10^{-7}*
Lateral diffusion from Pine Island Glacier including phytoplankton uptake	6.6 × 10^{-5}, 3.1 × 10^{-5}, 3.1 × 10^{-6} For 40, 70 and 159 km, respectively	*4.4 × 10^{-3}, 2.7 × 10^{-3}, 6.6 × 10^{-4} For 40, 70 and 159 km, respectively*
Lateral diffusion from Pine Island Glacier excluding phytoplankton uptake	8.8 × 10^{-5}, 5.3 × 10^{-5}, 1.2 × 10^{-5} For 40, 70 and 159 km, respectively	

Author's personal copy

2006), (4) sea ice melt (Lannuzel et al., 2007, 2008), and (5) glacial melt combined with lateral transport (Staham et al., 2008). Each of their potential contributions to the total Fe requirement of the *P. antarctica* bloom is assessed below.

4.2.2. Upwelling of MCDW in the PIP

The position of the ACC, in combination with a persistent clockwise wind field, causes upwelling in the Amundsen Sea and PIB (Assman and Timmermann, 2005). Giulivi and Jacobs (1997) defined Θ–S properties of the CDW in this part of the Southern Ocean by which we can recognize that the water flowing onto the shelf from the direction of st 3 brings CDW ($\Theta \leq 2$ °C and S_A=34.2–34.7 g kg^{-1}) that has been modified (MCDW, lower Θ, higher S) onto the shelf and into PIB (Fig. 3B). Since the MCDW flows into the Amundsen Sea over the sediment and through the deeper channels, the sediment is likely to be a source of DFe and TDFe to the inflowing CDW as it is converted to MCDW. Enrichment of DFe in MCDW in the PIP by shelf sediments was apparent during our study by the increase in DFe concentrations from 0.16 nM at 300 m at st 160 to a mean of 0.4 nM at 300 m in the PIP (Fig. 5). We assume that 0.4 nM DFe is the concentration of the sediment-enriched, inflowing MCDW that contributed to the upwelling in the PIP and use this concentration to calculate the DFe flux due to upwelling, as was done by Löscher et al. (1997), De Baar et al. (1995), Croot et al. (2004), and Klunder et al. (2011). According to Assman and Timmermann (2005), the maximum upwelling velocity in the Amundsen Sea obtained from a 44-year mean is 1×10^{-3} m d^{-1}. This results in a maximum upwelling flux of DFe in the PIP of 4×10^{-8} mol DFe m^{-2} d^{-1} (Table 2), in good agreement with the fluxes of 9.1×10^{-8} mol DFe m^{-2} d^{-1} for the Zero Meridian in the ACC (46–55°S) and 5.7×10^{-8} mol DFe m^{-2} d^{-1} in the Weddell Gyre calculated by Klunder et al. (2011). Results from Watson (2001) for the ACC of 1.2×10^{-7} mol DFe m^{-2} d^{-1} and De Baar et al. (1995) for the Atlantic sector of the ACC of 1.3×10^{-7} mol DFe m^{-2} d^{-1} are comparable, although higher. The estimated maximum upwelling flux in the PIP of 4×10^{-8} mol DFe m^{-2} d^{-1} would contribute only 0.4–1.7% of the Fe required to sustain the *P. antarctica* bloom.

The possible contribution of TDFe by upwelling is not well known. TDFe concentrations increased from around 0.5 nM at st 160 to 5 nM in the PIP (Fig. 5). It is often assumed that the upwelling flux of TDFe is twice that of DFe (De Baar et al., 1999; Sedwick et al., 2005; Lannuzel et al., 2007). However, since TDFe is mostly in particulate form that tends to sink out of the surface layer, upwelling of this fraction back to the surface is unlikely and will depend on the size of the particles. Given that typical particle sinking speeds are 8.6–86 m d^{-1} (10^{-4}–10^{-3} m s^{-1}), at least 100 times larger than the maximum upwelling velocities (Lampitt et al., 1993; van Haren et al., 1998), the contribution of TDFe to the *P. antarctica* bloom via upwelling is likely to be very small and will be neglected here.

4.2.3. Vertical diffusion

The maximum difference in DFe concentration over a depth of 275 m observed in the PIP during our study is 0.5 to 0.1 nM, giving a maximum vertical gradient (∂DFe/∂z) of 1.45 nM Fe m^{-1}. This is comparable to values measured by Blain et al. (2008) on the Kerguelen plateau. The vertical turbulent eddy diffusivity (K_z) that we estimated in the PIP varied considerably between stations (Table 1, Fig. 2). Stations 91, 102, and 104 had relatively high diffusivities of up to 293.8 m^2 d^{-1}, whereas st 14, 103, 105, and 106, and the stations in the Amundsen polynya, had quite low diffusivities of <8.6 m^2 d^{-1} ($<10^{-4}$ m^2 s^{-1}). Similar to values reported here, Blain et al. (2008) and Planquette et al. (2007) measured K_z values of 27.6 m^2 d^{-1} and 95 m^2 d^{-1}, respectively, on the Kerguelen Plateau and in the upper 300 m of the water column near the Crozet Islands (Fig. 2). Using the overall mean K_z of the PIP stations (62.2 m^2 d^{-1}, Table 2), we calculate the vertical diffusion of DFe in the polynya to be 9×10^{-8} mol DFe m^{-2} d^{-1}, sufficient to provide 1.0–3.8% of the Fe required by the *P. antarctica* bloom.

As was the case for upwelling, it is difficult to choose parameters for calculating the vertical diffusion of TDFe into the upper ocean. Using ∂DTFe/∂z=35.6 nM m^{-1} (concentration difference of 9.8 nM TDFe over 275 m), the flux would become 2.2×10^{-6} mol TDFe m^{-2} d^{-1}. Thus, vertical diffusion of TDFe would provide 24 to 92% of the Fe demand of the phytoplankton bloom in the PIP, but only if TDFe was fully available for phytoplankton uptake.

4.2.4. Dust

There are no known direct sources of dust in the vicinity of the Amundsen Sea. The mean dust flux in Antarctica is estimated by Edwards et al. (2006) to be 0.8×10^{-6} mol TDFe m^{-2} year^{-1} (3×10^{-9} mol m^{-2} d^{-1}). The solubility of Fe from dust depends on many factors, such as the distance from the source, processing during transport, presence of UV-radiation during transport and after deposition, bacterial activity, and residence time in the water (Baker and Croot, 2010; Boyd et al., 2010; and references therein). We assumed an upper limit for Fe solubility of 10%, based on data assembled by the above recent publications, which results in a flux of 3×10^{-10} mol DFe m^{-2} d^{-1}, less than 0.1% of the Fe requirement of the bloom (Table 2).

4.2.5. Sea ice melt

Sea ice surrounding the PIP and AP may serve as a source of DFe and TDFe as it melts in spring and summer. The maximum input of DFe and TDFe from melting sea ice can be calculated from the mean sea ice thickness (1.0 ± 0.32 m in the Bellinghausen Sea, Assmann et al., 2005) and winter concentrations of DFe and TDFe in sea ice of east Antarctica (18 nM DFe and 49 nM TDFe, respectively, Lannuzel et al., 2007). According to Lannuzel et al. (2010), the Fe content of pack ice and land fast ice is not spatially and temporally variable. Based on these assumptions, the maximum input from melting sea ice is 6.8×10^{-8} mol DFe m^{-2} d^{-1} and 1.8×10^{-7} mol TDFe m^{-2} d^{-1}. The flux of DFe from ice melt would be able to supply 0.7–2.9% of the bloom. How much TDFe will dissolve in the surface is unknown and again the estimation of TDFe flux is difficult to quantify.

It must be kept in mind that the flux from sea ice melt is temporally constrained since the polynyas usually open in November (Arrigo et al., 2012) through wind driven processes, potentially in combination with ice melt. Thus, the potential release of Fe from melting sea ice in the polynya is early in the bloom season and not spread over the year. On the other hand, a steady supply of multi-year sea ice is advected into the Amundsen Sea from the Bellinghausen Sea, thus providing a potential for a constant source of Fe at the northern edge of the polynya. The melting of icebergs was not taken into account, since we cannot quantify the presence of icebergs in the PIP.

4.2.6. Lateral turbulent diffusion from the glaciers

Vertical profiles of DFe and TDFe obtained at varying distances from the PIG (Figs. 5 and 6B) clearly showed that the PIG is a source of Fe. However, it is important to evaluate whether the elevated DFe and TDFe concentrations measured in these waters can be explained by melting glacier ice alone and if the PIG could be a source of Fe to the phytoplankton bloom in the PIP, the center of which was located 200 km away from the main source near the PIG.

Author's personal copy

To do so first requires calculation of the potential input of TDFe and DFe from melting of the PIG. According to Jacobs et al. (1996), the PIG releases 28 Gt (10^{12} kg) of freshwater each year into PIB. Raiswell et al. (2006) estimated that Antarctic glacial ice contains 1.0 kg of sediment per m^3 of glacial ice, 0.46–4.7% of which is highly reactive Fe (poorly ordered crystalline iron(oxy)hydroxes that can be extracted with a buffered (pH=4.8) sodium dithionite solution). Therefore, one liter of glacial ice should contain $0.09–0.86 \times 10^{-3}$ mol highly reactive particulate Fe. It is generally assumed that 90% of these particles will sink out of surface waters in the vicinity of the glacier (De Baar and De Jong, 2001; Raiswell et al., 2006).

The sea surface salinity at the front of the PIG (st 16) is at most 0.25 lower than that measured further offshore. Assuming that this reduction in salinity is due to glacial melt, we calculate that the surface waters near the PIG contain 0.7% (0.25/34.6=0.007) glacial melt water. Thus. 0.7% of the 10% remaining reactive particulate Fe (the fraction that did not sink) amounts to 59–602 nM TDFe that can be added to the upper water column by the melting of the PIG. If we assume that this highly reactive Fe is comparable to our measurements of TDFe, then the 27–105 nM TDFe measured at the front of the PIG (st 116 and 119) can be entirely attributed to glacier melting.

The concentrations of DFe in glacial ice are much less variable than TDFe concentrations, ranging from 20–50 nM (Raiswell et al., 2006). Thus, the 0.7% of glacial ice melt water near the PIG would increase DFe concentrations by 0.14–0.35 nM. This range is consistent with the observed increase in DFe in MCDW as it is upwelled to the surface in front of the PIG (0.23 nM DFe in deep MCDW at st 3 and 0.56 ± 0.18 nM DFe in meltwater MDCW, adjacent to the PIG). This provides strong support for the idea that the PIG is an important source of dissolved Fe for PIB.

To estimate the lateral turbulent diffusion of DFe and TDFe away from the PIG and into PIB and the PIP, we utilized the observed distribution of Fe in a transect perpendicular to the coast at increasing distances from the PIG (Fig. 7A,B and C). Fe concentrations decreased exponentially with distance from the PIG and were modeled following a dilution process assuming a single source, the glacier. The observed values were initially binned into several depth-layers (10, 25, 50 and 100 m) and assessed independently. However, the data in the upper 10–50 m showed virtually the same distributions, and thus these data were subsequently considered together (Fig. 7A and C), as was done by Planquette et al. (2007). Since phytoplankton are present in surface waters, the distribution of DFe in the upper 10–50 m is a function of both dilution and uptake by phytoplankton. However, phytoplankton concentrations at 100 m were very low so the distribution of DFe at that depth is assumed to be a function of dilution only, although some DFE is also removed by scavenging. Although TDFe distributions are not affected directly by phytoplankton uptake, some TDFe may dissolve as DFe concentrations decrease, since the organic ligands become more unsaturated with distance from the PIG (Thuróczy et al., 2012). However, TDFe is affected most strongly by removal over time via sinking particles. For the lateral turbulent flux calculation, the concentrations (C) of DFe and for TDFe are fit exponentially to the equation

$$C(x) = C_0 e^{-x/D} \tag{2}$$

where C_0 is the concentration at the front of the PIG, x is the distance from the PIG (m), and D is the scale length (m), defined as the distance where $C(x)=0.37C_0$ (i.e. the concentration has decreased to 37% of the initial concentration). For DFe, we find $[DFe]=0.6015e^{-x/39{,}000}$ ($R^2=0.72$, $n=26$, $D=39 \pm 11.6$ km, Fig. 7A) at 10–50 m and $[DFe]=0.5308e^{-x/58{,}823}$ ($R^2=0.78$, $n=8$, $D=58.8 \pm 18.0$ km, Fig. 7B) at 100 m depth. For TDFe, $[TDFe]=25.27e^{-x/62{,}500}$ ($R^2=0.86$, $n=15$, $D=62.5 \pm 17.6$ km,Fig. 7C) at 10–50 m. A calculation for TDFe at 100 m was not possible due to a lack of TDFe data at that depth.

The value of 39 ± 11.6 km obtained for D at 10–50 m for DFe is larger than the values of 16 km and 25 km found in surface mixed layer of Monterey Bay and upper 50 m near the Crozet Islands, respectively (Johnson et al., 1997; Planquette et al., 2007), but smaller than the value of 131 km measured at 40 depth m near the Kerguelen Islands (Bucciarelli et al., 2001). Ardelan et al. (2010) calculated scale lengths for depths <50 m near the Antarctic Peninsula of 25 and 12 km, respectively, for DFe and TDFe.

The scale length for TDFe is expected to be smaller than that for DFe due to greater loss of TDFe to sinking. However, at 10–50 m, we calculated a larger scale length for TDFe than that for DFe. This is likely due to uptake of DFe by phytoplankton. Consistent with this interpretation, the scale length for DFe at 100 m depth is similar to that of DFe at 10–50 m. In addition to biological processes, differences in scale length can also be attributed to differences in circulation, geochemical characteristic of the source area, and the type of continental shelf and margin (Ardelan et al., 2010).

Once D has been determined, we can use Okubo's (1971) parameterization to estimate horizontal turbulent diffusivity (K_h, $m^2\ s^{-1}$)

$$K_h = 7.3 \times 10^{-4} D^{1.15} \tag{3}$$

in which a 95% reduction length-scale l is used, $l=3D$.

The horizontal turbulent flux is then calculated as

$$F = K_h \partial C/\partial x, \tag{4}$$

or

$$F(x) = -7.3 \times 10^{-4} D^{0.15} C(x). \tag{5}$$

For distances from the glacier of $x=40$ km (st 99 in the central PIB), $x=70$ km (st 102 at the southern end of the PIP), and $x=159$ km (st 105 in the center of the PIP), DFe concentrations were 0.22 nM,

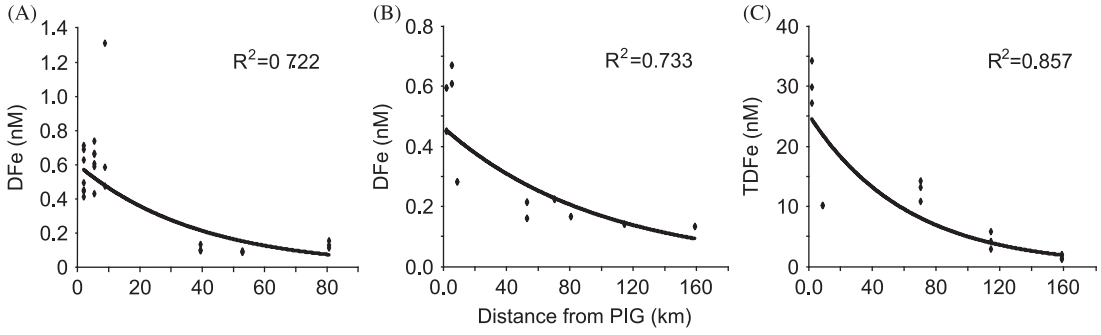

Fig. 7. Concentrations of dissolved Fe (DFe) at 10–50 m from stations 14, 16, 23, 55, 88, 89, 92, 93 and 99 ($n=26$) (A), DFe at 100 m from stations 14, 16, 23, 55, 88, 89, 92, 93 ($n=8$) (B), and total dissolvable Fe (TDFe) at 10–50 m from stations 16, 55, 102, 104 and 105 ($n=15$) (C). The black line represents the exponential fit of the data.

Author's personal copy

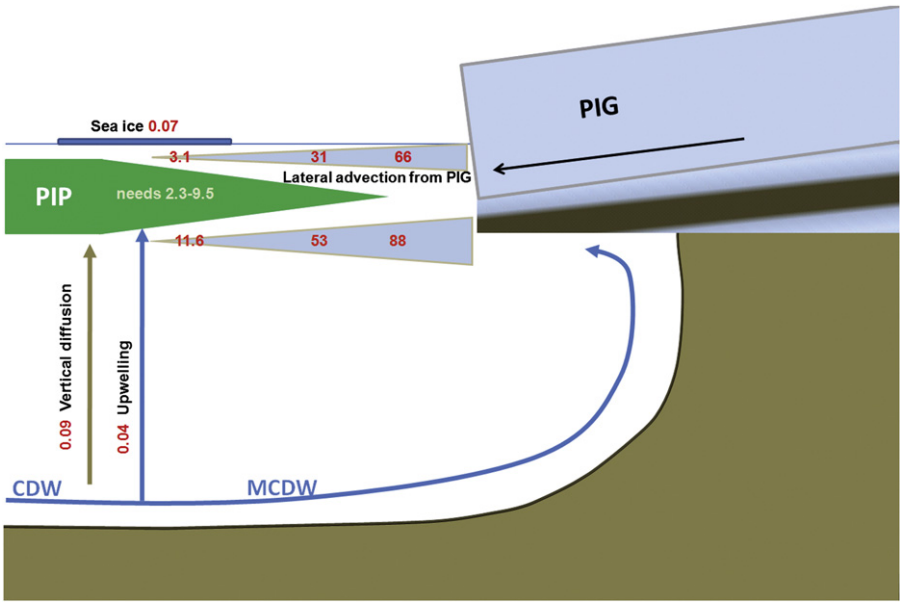

Fig. 8. Conceptual model of the fluxes of DFe ($\times 10^{-6}$ mol m^{-2} d^{-1}) fueling the phytoplankton bloom in the PIP. The Fe requirement of the phytoplankton bloom in the PIP is indicated in green. Two fluxes from the PIG are indicated, representing a surface (10–50 m) flux that includes Fe uptake by phytoplankton between the DFe source at the PIG, and a deep flux (100 m) where no DFe is taken up by phytoplankton. Numbers of the lateral fluxes (from left to right) are for the positions of stations 99, 102 and 105, respectively.

0.1 nM and 0.01 nM at 10–50 m and 0.27 nM, 0.16 nM and 0.04 nM at 100 m, respectively, according to the relationships in Eq. (2) (Fig. 7A and B). Thus, the horizontal fluxes of DFe at the three locations are $|F(40\,km)| = 6.7 \times 10^{-5}$ mol m^{-2} d^{-1} at 10–50 m depth and 8.6×10^{-5} mol m^{-2} d^{-1} at 100 m depth and $|F(70\,km)| = 3.1 \times 10^{-5}$ mol m^{-2} d^{-1} at 10–50 m depth and 5.3×10^{-5} mol m^{-2} d^{-1} and $|F(159\,km)| = 3.1 \times 10^{-6}$ mol m^{-2} d^{-1} at 10–50 m and 1.2×10^{-5} mol m^{-2} d^{-1} at 100 m depth. These are very large fluxes of DFe compared to the other sources and are large enough to sustain the observed phytoplankton bloom. At st 105 (159 km from the PIG), this flux can supply 34–131% of the requirement of the bloom at 10–50 m depth and 127–489% at 100 m depth, the range depending on the distance from the PIP (Fig. 8, Table 2).

The decrease in DFe with distance from the PIG in surface waters is also influenced by DFe uptake by phytoplankton and not solely due to dilution. Therefore, estimates of D made using DFe data from 10–50 m are probably too small. However, even using these underestimated values for D in Eq. (4) resulted in fluxes of DFe that were sufficiently high to fully support the Fe requirements of the *P. antarctica* bloom in the PIP.

Similarly, we find that for TDFe, $D = 6.4 \times 10^4$ m ($R^2 = 0.704$, $n = 18$) and that horizontal fluxes at 40 km and 70 km from the PIG are $|F(40\,km)| = 2.8 \times 10^{-3}$ mol m^{-2} d^{-1} and $|F(70\,km)| = 4.4 \times 10^{-3}$ mol m^{-2} d^{-1} and $|F(159\,km)| = 6.6 \times 10^{-4}$ mol m^{-2} d^{-1}. However, as was the case for the fluxes due to upwelling and the vertical eddy diffusivity, it is difficult to assess the effect of lateral turbulent flux on TDFe. The observed decrease in TDFe with a relatively large scale length is not caused by dilution alone. TDFe near the glacier consists primarily of inorganic material while in the polynya it consists mainly of biogenic material. Thuróczy et al. (2012) measured the organic complexation of DFe in these waters and found that stations near the glacier contained almost saturated ligands whereas nearer to and in the polynya, the ligands were undersaturated. These ligands can bind Fe released from the particulate phase, stimulate dissolution (Borer et al., 2005), and thus supply a more bio-available form of Fe to the phytoplankton. Another pathway for DFe might be dissolution of TDFe by photoreduction (Wells et al., 1991; Johnson et al., 1994; Waite et al., 1995; Rijkenberg et al., 2005, 2006) and complexation after re-oxidation. It has been hypothesized that the presence of icebergs stimulates phytoplankton blooms where dissolving particulate Fe is estimated to be the source (Smith et al., 2007; Schwarz and Schodlock, 2009; Raiswell et al., 2008; Raiswell, 2011). Fitzwater et al. (2000) suggested that the presence of resuspended particulate Fe in the Ross Sea produced conditions suitable for the development of phytoplankton blooms. Although it is difficult to quantify, TDFe might play an important role as source of Fe for phytoplankton in the PIP.

5. Conclusions

The bloom of predominantly *P. antarctica* lasted more than two months and apparently the flux of Fe was sufficient to support this. We estimated the DFe uptake rate by the bloom in the PIP using primary production and biomass as $7 \pm 5 \times 10^{-6}$ mol m^{-2} d^{-1}. The range in this estimate depends especially on the Fe:C ratio used, as values in the literature vary considerably (by a factor of 40).

We concluded that the increase of DFe and TDFe in the inflowing MCDW from 0.2 to 0.4 nM DFe and from 4 to 7–14 nM TDFe is due to Fe fluxes from the sediment. A further increase to 0.57 nM DFe and 22.4–38 nM TDFe was observed near the glaciers. In particular, near the glaciers, TDFe concentrations (up to 100 nM) were extremely high compared to concentrations found elsewhere. These high concentrations could be attributed to release of DFe and TDFe by glacier melt.

Upwelling of MCDW in the PIP could account for 0.4–1.7% of DFe needed by the phytoplankton bloom, vertical eddy diffusion could add 1.0–3.8%, and sea ice melt could contribute up to 2.9%. The lateral turbulent diffusion of DFe from the PIG to the middle of the PIP could account for 34–131% of the DFe requirements in the upper mixed layer, making it the biggest source of DFe and the likely explanation for the bloom's persistence.

The effect of glacier Fe source reached to a distance of 100–150 km and thus has here a local influence. However, lateral transport can be increased to distances over 300 km by currents as the Oyashio current in the Western Subarctic Pacific (Nishioka et al., 2011). Further studies are recommended with Southern Ocean models to arrive at a large scale quantification.

Author's personal copy

The role of TDFe as source for phytoplankton growth is unclear, although concentrations were very high, especially near the glaciers. Accurate calculation of TDFe fluxes is difficult because it is not known which fraction of the particulate Fe pool is involved in upwelling and diffusion. TDFe could be an important Fe source where solubilization by a combination of photoreduction and complexation is possible.

Acknowledgments

The authors are most grateful to the Captain and crew of R.V. *Nathaniel B. Palmer*, as well as to Stanley Jacobs, chief scientist during the NBP09-01 cruise. Frank Nitsche from Colombia University is thanked for making Fig. 1 and Nelleke Krijgsman (NIOZ) is acknowleged for improving the other figures. Ira van den Broek (NIOZ) is thanked for putting the data online. We thank the two anonynous reviewers for their constuctive remarks. The US component of this research was sponsored by the National Science Foundation Office of Polar Programs (DynaLiFe Grant ANT-0732535 to K.R. Arrigo) as part of the United States-International Polar Year program. The Dutch component was funded by NWO Geotraces sub-project (Grant 851.40.10) to H.J.W. de Baar and a NWO-NAAP Grant (851.20.041) to A.-C. Alderkamp.

References

Alderkamp, A.-C., Mills, M.M., van Dijken, G.L., Laan, P., Thuróczy, C.-E., Gerringa, L.J.A., de Baar, H.J.W., Payne, C., Tortell, P., Visser, R.J.W., Buma, A.,.G.J., Arrigo, K.R., 2012. Iron from melting glaciers fuels phytoplankton blooms in Amundsen Sea (Southern Ocean); phytoplankton characteristics and productivity. Deep-Sea Res. II 71–76, 32–48.

Ardelan, M.V., Holm-Hansen, O., Hewes, C.D., Reiss, C.S., Silva, N.S., Dulaiova, H., Steinnes, E., Sakshaug, E., 2010. Natural iron enrichment around the Antarctic Peninsula in the Southern Ocean. Biogeosciences 7 (11–25), 2010.

Arrigo, K.R., van Dijken, G.L., 2003. Phytoplankton dynamics within 37 Antarctic coastal polynya systems. J. Geophys. Res. 108 (C8), 3271. http://dx.doi.org/:10.1029/2002JC001739.

Arrigo, K.R., DiTullio, G.R., Dunbar, R.B., Lizotte, M.P., Robinson, D.H., VanWoert, M., Worthen, D.L., 2000. Phytoplankton taxonomic variability and nutrient utilization and primary production in the Ross Sea. J. Geophys. Res. 105, 8827–8846.

Arrigo, K.R., Worthen, D.L., Robinson, D.H., 2003. A coupled ocean-ecosystem model of the Ross Sea: 2. Iron regulation of phytoplankton taxonomic variability and primary production. J. Geophys. Res. 108 (C7), 3231. http://dx.doi.org/:10.1029/2001JC000856.

Arrigo, K.R., van Dijken, G.L., Bushinsky, S., 2008a. Primary production in the Southern Ocean, 1997–2006. J. Geophys. Res. 113, C08004. http://dx.doi.org/:10.1029/2007JC004551.

Arrigo, K.R., van Dijken, G., Long, M., 2008b. Coastal Southern Ocean: a strong anthropogenic CO_2 sink. Geophys. Res. Lett. 35, L21602. http://dx.doi.org/:10.1029/2008GL035624.

Arrigo, K.R., Lowry, K., van Dijken, G., 2012. Dynamics of sea ice and phytoplankton in polynyas of the Amundsen Sea, Antarctica. Deep-Sea Res. II 71–76, 5–15.

Assman, K.M., Timmermann, R., 2005. Variability of dense water formation in the Ross Sea. Ocean Dyn. 55, 68–87. http://dx.doi.org/:10.1007/s10236-004-0106-7.

Assmann, K.M., Hellmer, H.H., Jacobs, S.S., 2005. Amundsen Sea ice production and transport. J. Geophys. Res. 110, C12013. http://dx.doi.org/:10.1029/2004JC002797.

Baker, A.R., Croot, P.L., 2010. Atmospheric and marine controls on aerosol iron solubility in seawater. Mar. Chem. 120, 4–13.

Barbeau, K., Moffett, J.W., 2000. Laboratory and field studies of colloidal iron oxide dissolution as mediated by phagotrophy and photolysis. Limnol. Oceanogr. 45, 827–835.

Bergquist, B.A., Wu, J., Boyle, E.A., 2007. Variability in oceanic dissolved iron is dominated by the colloidal fraction. Geochim. Cosmochim. Acta 71, 2960–2974.

Blain, S., Quéguigiener, B., Armand, L., Belviso, S., Bombled, B., Bopp, L., Bowie, A., Brunet, C., Brussaard, C., Carlotti, F., Christaki, U., Corbière, A., Durand, I., Ebersbach, F., Fuda, J.-L., Garcia, N., Gerringa, L., Griffiths, B., Guigue, C., Guillerm, C., Jacquet, S., Jeandel, C., Laan, P., Lefèvre, D., Lomonaco, C., Malits, A., Mosseri, J., Obernosterer, I., Park, Y.-H., Picheral, M., Pondaven, P., Remenyi, T., Sandroni, V., Sarthou, G., Savoye, N., Scouarnec, L., Souhaut, M., Thuiller, D., Timmermans, K., Trull, T., Uitz, J., van-Beek, P., Veldhuis, M., Vincent, D., Viollier, E., Vong, L., Wagener, T., 2007. The effect of natural iron fertilization on carbon sequestration in the Southern Ocean. Nature 446, 1070–1075.

Blain, S., Sarthou, G., Laan, P., 2008. Distribution of dissolved iron during the natural iron fertilisation experiment KEOPS (Kerguelen Plateau, Southern Ocean). Deep-Sea Res. II 55, 594–605.

Borer, P.M., Sulzberger, B., Reichard, P., Kraemer, S.M., 2005. Effect of siderophores on the light-induced dissolution of colloidal iron(III) (hydr)oxides. Mar. Chem. 93, 179–193.

Boyd, P.W., Mackie, D.S., Hunter, K.A., 2010. Aerosol iron deposition to the surface ocean—modes of iron supply and biological responses. Mar. Chem. 120, 128–143.

Boye, M., van den Berg, C.M.G., de Jong, J.T.M., Leach, H., Croot, P.L., de Baar, H.J.W., 2001. Organic complexation of iron in the Southern Ocean. Deep-Sea Res. I 48, 1477–1497.

Buma, A.G.J., de Baar, H.J.W., Nolting, R.F., van Bennekom, A.J., 1991. Metal enrichment experiments in the Weddell–Scotia Seas: effects of Fe and Mn on various plankton communities. Limnol. Oceanogr. 36, 1865–1878.

Bucciarelli, E., Blain, S., Tréguer, P., 2001. Iron and manganese in the wake of the Kerguelen Islands (Southern Ocean). Mar. Chem. 73, 21–36.

Coale, K.H., et al., 1996. A massive phytoplankton bloom induced by an ecosystem-scale iron fertilisation experiment in the equatorial Pacific Ocean. Nature 383, 495–501.

Croot, P.L., Johansson, M., 2000. Determination of iron speciation by cathodic stripping voltammetry in seawater using the competing ligand 2-(2-Thiazolylazo)-p-cresol (TAC). Electroanalysis 12 (8), 565–576.

Croot, P.L., Andersson, K., Öztürk, M., Turner, D.R., 2004. The distribution and speciation of iron along 6°E in the Southern Ocean. Deep-Sea Res. II 51 (22–24), 2857–2879.

De Baar, H.J.W., De Jong, J.T.M., 2001. Distributions, sources and sinks of iron in seawater. In: Turner, D., Hunter, K. (Eds.), The Biogeochemistry of Iron in Seawater, IUPAC Book Series on Analytical and Physical Chemistry of Environmental Systems, vol. 7. John Wiley and Sons Ltd., Chichester, pp. 123–253.

De Baar, H.J.W., Buma, A.G.J., Nolting, R.F., Cadée, G.C., Jacques, G., Tréguer, P.J., 1990. On iron limitation of the Southern Ocean: experimental observations in the Weddell and Scotia Seas. Mar. Ecol. Prog. Ser. 65, 105–122.

De Baar, H.J.W., De Jong, J.T.M., Bakker, D., Löscher, B.M., Veth, C., Bathmann, U., Smeteck, V., 1995. Importance of iron for phytoplankton spring blooms and CO_2 drawdown in the Southern Ocean. Nature 373, 412–415.

De Baar, H.J.W., De Jong, J.T.M., Nolting, R.F., Timmerman, K.R., van Leeuwe, M.A., Bathmann, U., Rutgers van der Loeff, M., Sildam, J., 1999. Low dissolved Fe and the absence of diatom blooms in remote Pacific waters of the Southern Ocean. Mar. Chem. 66, 1–34.

De Baar, H.J.W., Timmermans, K.R., Laan, P., De Porto, H.H., Ober, S., Blom, J.J., Bakker, M.C., Schilling, J., Sarthou, G., Smit, M.G., Klunder, M., 2008a. Titan: a new facility for ultraclean sampling of trace elements and isotopes in the deep oceans in the international Geotraces program. Mar. Chem. 111 (1–2), 4–21.

De Baar, H.J.W., Gerringa, L.J.A., Laan, P., Timmermans, K.R., 2008b. Efficiency of carbon removal per added iron in ocean fertilization. Theme section "implications of large-scale iron fertilization of the oceans". Mar. Ecol. Prog. Ser. 364, 269–282.

De Jong, J.T.M., Den Das, J., Bathmann, U., Stoll, M.H.C., Kattner, G., Nolting, R.F., De Baar, H.J.W., 1998. Dissolved iron at subnanomolar levels in the Southern Ocean as determined by ship-board analysis. Anal. Chim. Acta 377, 113–124.

Dillon, T.M., 1982. Vertical overturns: a comparison of Thorpe and Ozmidov length scales. J. Geophys. Res. 87, 9601–9613.

Edwards, R., Sedwick, P., 2001. Iron in East Antarctic snow: implications for atmospheric iron deposition and algal production in Antarctic waters. Geophys. Res. Lett. 28, 3907–3910.

Edwards, R., Sedwick, P., Morgan, V., Boutron, C., 2006. Iron in ice cores from Law Dome: a record of atmospheric iron deposition for maritime East Antarctica during the Holocene and Last Glacial Maximum. Geochem., Geophys., Geosyst., 7. http://dx.doi.org/:10.1029/2006GC001307.

Fichefet, T., Tartinville, B., Goosse, H., 2003. Antarctic sea ice variability during 1958–1999: a simulation with a global ice-ocean model. J. Geophys. Res. 108 (C3).

Fitzwater, S.E., Johnson, K.S., Gordon, R.M., Coale, K.H., Smith Jr., W.O., 2000. Trace metal concentrations in the Ross Sea and their relationship with nutrients and phytoplankton growth. Deep-Sea Res. II 47, 3159–3179.

Gerringa, L.J.A., de Baar, H.J.W., Timmermans, K.R., 2000. A comparison of iron limitation of phytoplankton in natural oceanic waters and laboratory media conditioned with EDTA. Mar. Chem. 68, 335–346.

Gerringa, L.J.A., Rijkenberg, M.J.A., Wolterbeek, H.Th., Verburg, T., Boye, M., de Baar, H.J.W., 2007. Kinetic study reveals weak Fe-binding ligand, which affects the solubility of Fe in the Scheldt estuary. Mar. Chem. 103, 30–45.

Giulivi, C.F., Jacobs, S.S., 1997. Oceanographic Data in the Amundsen and Bellingshausen Seas. N.B. *Palmer cruise* 9402, February–March 1994. Technical Report LDEO-97-3. Lamont-Doherty Earth Obs. of Columbia Univ., Palisades, N.Y., 330 pp.

Gledhill, M., van den Berg, C.M.G., 1994. Determination of complexation of iron (III) with natural organic complexing ligands in seawater using cathodic stripping voltammetry. Mar. Chem. 47, 41–54.

Grotti, M., Soggia, F., Ianni, C., Frache, R., 2005. Trace metals distributions in coastal sea ice of Terra Nova Bay, Ross Sea, Antarctica. Antarct. Sci. 17 (2), 289–300.

Hassler, C.S., Schoemann, V., 2009. Bioavailability of organically bound Fe to model phytoplankton of the Southern Ocean. Biogeosci. Discussion 6, 1677–1712.

Hellmer, H.H., 2004. Impact of Antarctic ice shelf basal melting on sea ice and deep ocean properties. Geophys. Res. Lett. 31, L10307. http://dx.doi.org/:10.1029/2004GL019506.

Hosegood, P., Haren, H., van, Veth, C., 2005. Mixing within the interior of the Faeroe-Shetland Channel. J. Mar. Res. 63, 529–561.

Jacobs, S.S., Comiso, J.C., 1997. Climate variability in the Amundsen and Bellingshausen sea. J. Clim. 10, 697–709.

Author's personal copy

Jacobs, S.S., Hellmer, H.H., Jenkins, A., 1996. Antarctic ice sheet melting in the southeast Pacific. Geophys. Res. Lett. 23, 957–960.
Jacobs, S.S., Jenkins, A., Giuivi, C.F., Dutrieux, P., 2011. Stronger ocean circulation and increased melting under Pine Island Glacier ice shelf. Nat. Geosci. 4, 519–523. http://dx.doi.org/:10.1038/NGEO1188.
Jenkins, A., Vaughan, D.G., Jacobs, S.S., Hellmer, H.H., Keys, J.R., 1997. Glaciological and oceanographic evidence of high melt rates beneath Pine Island Glacier, West Antarctica. J. Glaciol. 43, 114–121.
Jenkins, A., Dutrieux, P., Jacobs, S.S., McPhail, S.D., Perrett, J.R., Webb, A.T., White, D., 2010. Observations beneath Pine Island Glacier in West Antarctica and implications for its retreat. Nat. Geosci. 3, 468–472. http://dx.doi.org/:10.1038/NGEO890.
Jickells, T.D., Spokes, L.J., 2001. Atmospheric iron inputs to the oceans. In: Turner, D.R., Hunter, K. (Eds.), The Biogeochemistry of Iron in Seawater. Wiley, Chichester, pp. 85–121.
Johnson, K.S., Coale, K.H., Elrod, V.A., Tindale, N.W., 1994. Iron photochemistry in waters from the equatorial Pacific. Mar. Chem. 46, 319–334.
Johnson, K.S., Gordon, R.M., Coale, K.H., 1997. What controls dissolved iron concentrations in the world ocean? Mar. Chem. 57, 137–161.
Johnson, K.S., Boyle, E., Bruland, K., Measures, C., Moffett, J., Aquilarislas, A., Barbeau, K., Cai, Y., Chase, Z., Cullen, J., Doi, T., Elrod, V., Fitzwater, S., Gordon, M., King, A., Laan, P., Laglera-Baquer, L., Landing, W., Lohan, M., Mendez, J., Milne, A., Obata, H., Ossiander, L., Plant, J., Sarthou, G., Sedwick, P., Smith, G.J., Sohst, B., Tanner, S., Van Den Berg, S., Wu, J., 2007. Developing standards for dissolved iron in seawater. Eos Trans. AGU 88 (11), 131.
Joughin, I., Rignot, E., Rosanova, C.E., Lucchitta, B.K., Bohlander, J., 2003. Timing of recent accelerations of Pine Island Glacier, Antarctica. Geophys. Res. Lett. 30, 1706.
Klunder, M., Laan, P., Middag, R., De Baar, H.J.W., van Ooijen, J., 2011. Dissolved Iron in the Southern Ocean (Atlantic Sector). Deep-Sea Res. II 58, 2678–2694.
Kuma, K., Nishioka, J., Matsunaga, K., 1996. Controls on iron(III) hydroxide solubility in seawater: the influence of pH and natural organic chelators. Limnol. Oceanogr. 41 (1996), 396–407.
Kuma, K., Katsumoto, A., Shiga, N., Sawabe, T., Matsunaga, K., 2000. Variation of size-fractionated Fe concentrations and Fe(III)hydroxide solubilities during a spring phytoplankton bloom in Funka Bay (Japan). Mar. Chem. 71, 111–123.
Lampitt, R.S., Hillier, W.R., Challenor, P.G., 1993. Seasonal and diel variation in the open ocean concentration of marine snow aggregates. Nature 362, 737–739.
Lannuzel, D., Schoemann, V., de Jong, J.T.M., Tison, J.-L., Chou, L., 2007. Distribution and biogeochemical behaviour of iron in the East Antarctic sea ice. Mar. Chem. 106, 18–32.
Lannuzel, D., Chou, J.T.M., Delille, L., Becquevort, B., Tison, J.-L., S., 2008. Iron study during a time series in the western Weddell pack ice. Mar. Chem. 108 (1–2), 85–95.
Lannuzel, D., Schoemann, V., De Jong, Pasquer, B., van der Merwe, P., Masson, F., Tison, J.-L., Bowie, A., 2010. Distribution of dissolved iron in Antarctic sea ice: spatial, seasonal, and inter-annual variability. J. Geophys. Res. 115, G03022. http://dx.doi.org/:10.1029/2009JG001031.
Lin, H., Rauschenberg, S., Hexel, C.R., Shaw, T.J., Twining, B.S., 2011. Free-drifting icebergs as sources of iron to the Weddell Sea. Deep-Sea Res. II 58, 1392–1406.
Liu, X., Millero, F.J., 2002. The solubility of iron in seawater. Mar. Chem. 77, 43–54.
Löscher, B.M., De Baar, H.J.W., De Jong, J.T.M., Veth, C., Dehairs, F., 1997. The distribution of Fe in the Antarctic Circumpolar Current. Deep-Sea Res. II 44, 143–187.
Mankoff, K.D., Jacobs, S.S., Tulaczyk, S.M., Stammerjohn, S.E., 2012. The role of Pine Island Glacier ice shelf basal channels in deep-water upwelling, polynyas and ocean circulation in Pine Island Bay, Antarctica. Ann. Glaciol. 53, 123–128.
Martin, J.H., Coale, K.H., Johnson, K.S., Fitzwater, S.E., Gordon, R.M., Tanner, S.J., Hunter, C.N., Elrod, V.A., Nowicki, J.L., Coley, T.L., Barber, R.T., Lindley, S., Watson, A.J., van Scoy, K., Law, C.S., Liddicoat, M.I., Ling, R., Station, T., Stockel, J., Collins, C., Anderson, A., Bidigare, R., Ondrusek, M., Latasa, M., Millero, F.J., Lee, K., Yao, W., Zhang, J.Z., Friederich, G., Sakamoto, C., Chavez, F., Buck, K., Kolber, Z., Green, R., Falkowski, P., Chisholm, S.W., Hoge, F., Swift, R., Yangel, J., Turner, S., Nightingale, P., Hatton, A., Liss, P., Tindale, N.W., 1994. Testing the iron hypothesis in ecosystems of the equatorial Pacific Ocean. Nature 371, 123–129.
McDougall, T.J., Feistel, R., Millero, F.J., Jackett, D.R., Wright, D.G., King, B.A., Marion, G.M., Chen, C.-T.A., Spitzer, P., 2009. Calculation of the Thermodynamic Properties of Seawater. Global Ship-Based Repeat Hydrography Manual. IOCCP Report 14. ICPO Publ. Ser. 134, U.N.E.S.C.O., Paris, F., 131 pp.
Measures, C.I., Vink, S., 2001. Dissolved Fe in the upper waters of the Pacific sector of the Southern Ocean. Deep-Sea Res. II 48 (19–20), 3913–3941.
Measures, C.I., Landing, W.M., Brown, M.T., Buck, C.S., 2008. High-resolution Al and Fe data from the Atlantic Ocean CLIVAR-CO_2 Repeat Hydrography A16N transect: extensive linkages between atmospheric dust and upper ocean geochemistry. Global Biogeochem. Cycles 22, GB1005. http://dx.doi.org/:10.1029/2007GB003042.
Mills, M., Alderkamp, A.-C., Thurcózy, C.-E., van Dijken, G.L., Laan, P., de Baar, H.J.W., Arrigo, K.R., 2012. Phytoplankton biomass and pigment responses to Fe amendments in the Pine Island and Amundsen polynyas. Deep-Sea Res. II 71–76, 61–76.
Nishioka, J., Takeda, S., Wong, C.S., Johnson, W.K., 2001. Sizefractionated iron concentrations in the northeast Pacific Ocean: distribution of soluble and small colloidal iron. Mar. Chem. 74, 157–179.
Nishioka, J., Takeda, S., Kudo, I., Tsumune, D., Yoshimura, T., Kuma, K., Tsuda, A., 2003. Size-fractionated iron distributions and iron-limitation processes in the subarctic NW Pacific. Geophys. Res. Lett. 30 (14), 1730. http://dx.doi.org/:10.1029/2002GL016853.
Nishioka, J., Ono, T., Saito, H., Sakaoka, K., Yoshimura, T., 2011. Oceanic iron supply in the Oyashio region, western subarctic Pacific. J. Geophys. Res. 116, 1–17. http://dx.doi.org/:10.1029/2010JC006321.
Okubo, A., 1971. Oceanic diffusion diagrams. Deep-Sea Res. 18 (1971), 789–802.
Park, Y.-H., Fuda, J.-L., Durand, I., Naveira Garabato, A.C., 2008. Internal tides and vertical mixing over the Kerguelen Plateau. Deep-Sea Res. II 55, 582–593.
Planquette, H., Statham, P.J., Fones, G.R., Charette, M.A., Moore, C.M., Salter, I., Nédélec, F.H., Taylor, S.L., French, M., Baker, A.R., Mahowald, N., Jickells, T.D., 2007. Dissolved iron in the vicinity of the Crozet Islands, Southern Ocean. Deep-Sea Res. II, 1999–2019.
Raiswell, R., 2011. Iceberg-hosted nanoparticulate Fe in the Southern Ocean: mineralogy, origin, dissolution kinetics and source of bioavailable Fe. Deep-Sea Res. II 58, 1364–1375.
Raiswell, R., Tranter, M., Benning, L.G., Siegert, M., Death, R., Huybrechts, P., Payne, T., 2006. Contributions from glacially derived sediment to the global iron (oxyhydr)oxide cycle: implications for iron delivery to the oceans. Geochim. Cosmochim. Acta 70, 2765–2780.
Raiswell, R., Benning, L.G., Tranter, M., Tulaczyk, S., 2008. Bioavailable iron in the Southern Ocean: the significance of the iceberg conveyor belt. Geochem. Trans. 9 (7). http://dx.doi.org/:10.1186/1467-4866-9-7.
Rignot, E., 2008. Changes in West Antarctic ice stream dynamics observed with ALOS PALSAR data. Geophys. Res. Lett. 35, L12505.
Rue, E.L., Bruland, K.W., 1997. The role of organic complexation on ambient iron chemistry in the equatorial Pacific Ocean and the response of a mesoscale iron addition experiment. Limnol. Oceanogr. 42, 901–910.
Rijkenberg, M.J.A., Fischer, A.C., Kroon, J.J., Gerringa, L.J.A., Timmermans, K.R., Wolterbeek, H.Th., de Baar, H.J.W., 2005. The influence of UV irradiation on the photoreduction of iron in the Southern Ocean. Mar. Chem. 93, 119–129.
Rijkenberg, M.J.A., Gerringa, L.J.A., Carolus, V.E., Velzeboer, I., de Baar, H.J.W., 2006. Enhancement and inhibition of iron photoreduction by individual ligands in open ocean seawater. Geochim., Cosmochim. Acta 70, 2790–2805.
Sarthou, G., Vincent, D., Christaki, U., Obernosterer, I., Timmermans, K.R., Brussaard, C.P.D., 2008. The fate of biogenic iron during a phytoplankton bloom induced by natural fertilization: impact of copepod grazing. Deep-Sea Res. II 55, 734–751.
Schoemann, V., Wollast, R., Chou, L., Lancelot, C., 2001. Effects of photosynthesis on the accumulation of Mn and Fe by Phaeocystis colonies. Limnol. Oceanogr. 46 (5), 1065–1076.
Schoemann, V., Becquevort, S., Stefels, J., Rousseau, V., Lancelot, C., 2005. Phaeocystis blooms in the global ocean and their controlling mechanisms: a review. J. Sea Res. 53 (43–66), 2005.
Schwarz, J.N., Schodlock, M.P., 2009. Impact of drifting icebergs on surface phytoplankton biomass in the Southern Ocean: ocean colour remote sensing and in situ iceberg tracking. Deep-Sea Res. I 56, 1727–1741.
Sedwick, P.N., DiTullio, G.R., Mackey, D.J., 2000. Iron and manganese in the Ross Sea, Antarctica: seasonal iron limitation in Antarctic shelf waters. J. Geophys. Res. 105 (C5), 11321–11336.
Sedwick, P.N., Church, T.M., Bowie, A.R., Marsay, C.M., Ussher, S.J., Achilles, K.M., Lethaby, P.J., Johnson, R.J., Sarin, M.M., McGillicuddy, D.J., 2005. Iron in the Sargasso Sea (Bermuda Atlantic time-series study region) during summer: eolian imprint, spatiotemporal variability, and ecological implications. Global Biogeochem. Cycles 19, GB4006.
Sedwick, P.N., Bowie, A.R., Trull, T.W., 2008. Dissolved iron in the Australian sector of the Southern Ocean (CLIVAR SR3 section); meridional and seasonal trends. Deep-Sea Res. I 55, 911–925.
Smith Jr., W.O., Carlson, C.A., Ducklow, H.W., Hansell, D.A., 1998. Growth dynamics of *Phaeocystis antarctica*-dominated plankton assemblages from the Ross Sea. MEPS 168, 229–244.
Smith, K.L., Robinson, B.H., Helly, J.J., Kaufmann, R.S., Ruhl, H.A., Shaw, T.J., Twining, B.S., Vernet, M., 2007. Free-drifting icebergs: hot spots of chemical and biological enrichment in the Weddell Sea. Science 317, 478–482.
Staham, P.J., Skidmore, M., Tranter, M., 2008. Inputs of glacially derived dissolved and colloidal iron to the coastal ocean and implications for primary productivity. Global Biogeochem. Cycles 22, GB3013. http://dx.doi.org/:10.1029/2007GB003106.
Stephenson, G.R., Sprintall, J., Gille, S.T., Vernet, M., Helly, J.J., Kaufmann, R.S., 2011. Subsurface melting of a free-floating Antarctic iceberg. Deep-Sea Res. II 58, 1336–1345.
Sunda, W.G., Huntsman, S.A., 1997. Interrelated influence of iron, light and cell size on marine phytoplankton growth. Nature 390, 389–392.
Strzepek, R.F., Maldonado, M.T., Hunter, K.A., Frew, R.D., Boyd, P.W., 2011. Adaptive strategies by Southern Ocean phytoplankton to lessen iron limitation: uptake of organically complexed iron and reduced cellular iron requirements. Limnol. Oceanogr. 56, 1983–2002.
Tagliabue, A., Arrigo, K.R., 2006. Processes governing the supply of iron to phytoplankton in stratified seas. J. Geophys. Res.—Oceans 111 (C6), C06019.
Tagliabue, A., Bopp, L., Dutay, J.-C., Bowie, A.R., Chever, F., Jean-Baptiste, P., Bucciarelli, E., Lannuzel, D., Remenyi, T., Sarthou, G., Aumont, O., Gehlen, M., Jeandel, C., 2010. Hydrothermal contribution to the oceanic dissolved iron inventory. Nat. Geosci. 14, 1–5. http://dx.doi.org/:10.1038/NGEO818.
Thompson, P.A., Guo, M., Harrison, P.J., 1992. Effects of variation in the temperature. I. On the biochemical composition of eight species of marine phytoplankton. J. Phycol. 28, 481–488.
Thorpe, S.A., 1977. Turbulence and mixing in a Scottish Loch. Philos. Trans. R. Soc. London Ser. A 286, 125–181.

Author's personal copy

Thuróczy, C.-E., Gerringa, L.J.A., Klunder, M., Middag, R., Laan, P., Timmermans, K.R., de Baar, H.J.W., 2010. Speciation of Fe in the North East Atlantic Ocean. Deep-Sea Res I 57, 1444–1453.

Thuróczy, C.-E., Gerringa, L.J.A., Klunder, M., Laan, P., de Baar, H.J.W., 2011. Observation of consistent trends in the organic complexation of dissolved iron in the Atlantic sector of the Southern Ocean. Deep-Sea Res. II 58, 2695–2706.

Thuróczy, C.-E., Alderkamp, A.-C., Laan, P., Gerringa, L.J.A., de Baar, H.J.W., Arrigo, K.R., 2012. Key role of organic complexation of iron in sustaining phytoplankton blooms in the Pine Island and Amundsen Polynyas (Southern Ocean). Deep-Sea Res. II 71–76, 49–60.

Twining, B.S., Baines, S.B., Fischer, N.S., Landry, M.R., 2004. Cellular iron contents of plankton during the Southern Ocean Iron Experiment (SOFeX). Deep-Sea Res. I 51, 1827–1850.

van Haren, H., Mills, D.K., Wetsteyn, L.P.M.J., 1998. Detailed observations of the phytoplankton spring bloom in the stratifying central North Sea. J. Mar. Res. 56, 655–680.

Waite, T.D., Szymczak, R., Espey, Q.I., Furnas, M.J., 1995. Die1 variations in iron speciation in northern Australian shelf waters. Mar. Chem. 50, 79–91.

Watson, A.J., 2001. Iron limitation in the oceans. In: Turner, D.R., Hunter, K.H. (Eds.), The Biogeochemistry of Iron in Seawater, vol. 7. IUPAC Series on Analytical and Physical Chemistry of Environmental Systems, pp. 9–39.

Wells, M.L., Mayer, L.M., Donard, O.F.X., de Souza Sierra, M.M., Ackleson, S., 1991. The photolysis of colloidal iron in the oceans. Nature 353, 248–250.